Computing real monodromy action

Jonathan D. Hauenstein[1*] Margaret H. Regan[2] Emma L. Schmidt[1†]
Charles W. Wampler[1‡]

[1]Department of Applied and Computational Mathematics and Statistics, University of Notre Dame, Notre Dame, IN 46556, {hauenstein,eschmi23,cwample1}@nd.edu

[2]Department of Mathematics, Grand Valley State University, Allendale, MI 49401, reganmar@gvsu.edu

Abstract

Over the complex numbers, the algebraically defined Galois group of a dominant map between irreducible complex varities of the same dimension corresponds with the geometric monodromy group. The Galois/monodromy group encodes subtle structure associated with the branched covering. One can similarly define monodromy behavior over the real numbers yielding the real monodromy group. Since it is often the case that the real monodromy group is trivial and thus does not capture structure present in the branched covering, the first and second authors proposed real monodromy action based on tiered behavior of individual collections of real solutions rather than the entire set of real solutions simultaneously. Since real monodromy action arises from smoothly connected semialgebraic sets, this paper describes an approach to compute real monodromy action using fiber products and routing functions. Several examples are included to demonstrate this computational approach, including an example in kinematics with various types of application-relevant leg length and packaging constraints.

Keywords. Galois group, monodromy group, real monodromy action, smoothly connected components, numerical algebraic geometry, real algebraic geometry

AMS Subject Classification. 65H14, 65H20, 14P99, 14Q99

1 Introduction

For irreducible algebraic sets $X \subset \mathbb{C}^N$ and $Y \subset \mathbb{C}^P$ with $\dim X = \dim Y$, a branched covering $\pi : X \to Y$ is a covering map except on a branch locus $B \subset Y$ where B is contained in a proper Zariski closed subset of Y. That is, the codimension of the branch locus in Y is at least one. Hence, when treating $\mathbb{C} \cong \mathbb{R}^2$, the real codimension is at least two so that real loops, which have real dimension equal to one, can be taken in Y that avoid B. Such a loop induces a permutation on the points in X above a fixed point on the loop, called a base point. The monodromy group is the group generated by all such permutations arising from loops in $Y \backslash B$ passing through a fixed base point, and is equal to the Galois group [6, 12]. Since $Y \backslash B$ is connected, the monodromy group is independent of the choice of base point and encodes subtle information [6, 17, 25].

*Supported in part by NSF CCF-2331440 and the Robert and Sara Lumpkins Collegiate Professorship.
†Supported in part by NSF CCF-2331400 and the Arthur J. Schmitt Presidential Leadership Fellowship.
‡Supported in part by the Huisking Foundation, Inc., Collegiate Professorship.

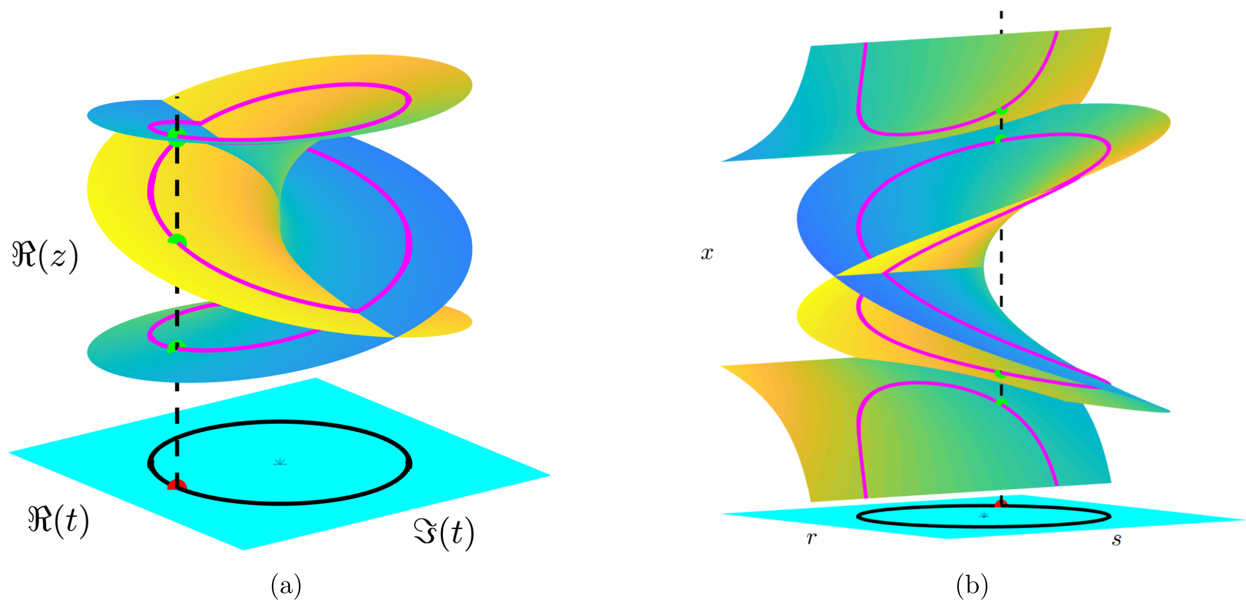

Figure 1: (a) Illustrating the cyclic monodromy group from $z^3 - t = 0$ in coordinates $(\Re(t), \Im(t), \Re(z))$ with surface colored by the value of $\Im(z)$ showing that the paths do not actually intersect in $\mathbb{C}^2$. (b) Illustrating a real monodromy action for G in (2) in coordinates (r, s, x) with the surface colored by the value of y showing that the paths do not actually intersect in $\mathbb{R}^4$.

As an illustrative example, let $f(z,t) = z^3 - t$ with $X = V_{\mathbb{C}}(f) = \{(z,t) \in \mathbb{C}^2 \mid f(z,t) = 0\} \subset \mathbb{C}^2$ and $Y = \mathbb{C}$. The projection map $\pi : V_{\mathbb{C}}(f) \to \mathbb{C}$ defined by $\pi(z,t) = t$ is a branched covering with branch locus $B = \{0\}$ in which the monodromy group is the cyclic group of order 3, $\mathbb{Z}_3$, as illustrated in Figure 1a. Numerical algebraic geometry (see the books [2,23] for a general overview) can be used to compute the monodromy group [9], while the monodromy group is also utilized to produce global [22] and local [4] numerical irreducible decompositions.

On one hand, it is quite natural to consider a real analogue of the monodromy group, yielding the real monodromy group. As pictorially demonstrated by Figure 1a, the monodromy group becomes the real monodromy group simply by treating $\mathbb{C} \cong \mathbb{R}^2$. That is, replacing z by $x + \mathrm{i}y$ and t by $r + \mathrm{i}s$ for $x, y, r, s \in \mathbb{R}$ and $\mathrm{i} = \sqrt{-1}$, the monodromy group for the illustrative example, $\mathbb{Z}_3$, is equal to the real monodromy group defined by the projection map $\pi(x, y, r, s) = (r, s)$ from $V_{\mathbb{R}}(F) = \{(x, y, r, s) \in \mathbb{R}^4 \mid F(x, y, r, s) = 0\}$ to $\mathbb{R}^2$ where F is obtained by taking real and imaginary parts of $f(x + \mathrm{i}y, r + \mathrm{i}s)$, namely,

$$F(x,y,r,s) = \begin{bmatrix} \Re(f(x+\mathrm{i}y, r+\mathrm{i}s)) \\ \Im(f(x+\mathrm{i}y, r+\mathrm{i}s)) \end{bmatrix} = \begin{bmatrix} x^3 - 3xy^2 - r \\ 3x^2y - y^3 - s \end{bmatrix}. \tag{1}$$

For every $(r^*, s^*) \in \mathbb{R}^2 \backslash \{(0,0)\}$, $F(x, y, r^*, s^*) = 0$ has 3 real solutions and any simple loop around the origin cyclically permutes them as expected by observing Figure 1a.

On the other hand, when considering real monodromy groups for problems which do not arise from using $\mathbb{C} \cong \mathbb{R}^2$, the branch locus can have real codimension one so that $Y \backslash B$ could decompose into different connected components. The real monodromy group is then dependent upon which connected component of $Y \backslash B$ the base point is selected from. Moreover, if the fundamental group of the connected component is trivial, i.e., every loop is contractible, then the corresponding real

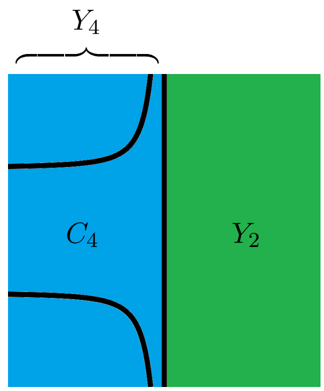

Figure 2: Illustration of B (black curves) with a decomposition of $\mathbb{R}^2\backslash B$ into four connected components with each having a trivial fundamental group. The left region (blue), Y_4, are parameters corresponding with 4 real solutions and the right region (green), Y_2, are parameters corresponding with 2 real solutions as specified in (10). Moreover, Y_4 has 3 connected components, one of which is C_4 defined in (11), while Y_2 is connected.

monodromy group is also trivial [8, Thm. 3.3]. For $\pi(x, y, r, s) = (r, s)$ from $V_{\mathbb{R}}(G)$ to $\mathbb{R}^2$ where

$$G(x, y, r, s) = \begin{bmatrix} (x^2 - y^2 - r)(rx^2 + 1) \\ 2xy - s \end{bmatrix}, \tag{2}$$

then $B = V_{\mathbb{R}}(r \cdot (r^2 s^2 - 4r^2 - 4)) \cap \{r \leqslant 0\}$ as shown in black in Figure 2. In particular, the fundamental group of each connected component of $\mathbb{R}^2\backslash B$ is trivial. Nonetheless, there is still structure of the real solutions present as two real solutions can interchange for a small loop around the origin as illustrated in Figure 1b.

In order to capture more information about the behavior of the real solutions, real monodromy action was introduced in [8] and describes tiered behavior of collections of real solutions. The first tier captures which of the real solutions can be smoothly connected to a real solution via a real loop. For example, if ℓ is a real loop such that the solution path starting at real solution α is smooth and ends at real solution β, we can describe such a tier one real monodromy action as $\alpha \xrightarrow{\ell} \beta$. If $\alpha \neq \beta$, then this is a nontrivial real monodromy action which, in kinematics, is called a nonsingular assembly mode change, e.g., see [5, 15, 16, 19, 26]. The real monodromy structure does not record the loop ℓ and succinctly encodes real monodromy action based on a global ordering of the real solutions, analogous to the monodromy group.

The second tier captures which ordered pairs of real solutions can be smoothly connected to an ordered pair of real solutions via a real loop. Continuing as above, if ℓ is a real loop such that the solution paths starting at distinct real solutions α_1 and α_2 are smooth ending at real solutions β_1 and β_2, respectively, we can describe such a tier two real monodromy action as $(\alpha_1, \alpha_2) \xrightarrow{\ell} (\beta_1, \beta_2)$. If $(\alpha_1, \alpha_2) \neq (\beta_1, \beta_2)$, then this is a nontrivial real monodromy action. Higher tiers of real monodromy action are defined similarly. For example, the Stephenson III six-bar linkage considered in [20, § 5] has a nonsingular assembly mode change obtained by rotating a crank one complete loop. Rotating the crank yields a loop ℓ and this describes a tier one real monodromy action of $\alpha \xrightarrow{\ell} \beta$ for certain distinct configurations α and β. However, the pair cannot be simultaneously smoothly interchanged since there is a singularity that arises when attempting to rotate the crank a second time, i.e., $(\alpha, \beta) \xrightarrow{\ell} (\beta, \alpha)$ is not a valid tier two real monodromy action. Such behavior can be observed using the depressed cubic summarized in Example 3.7 and illustrated in Figure 4.

The first and second tiers of real monodromy action are illustrated in Figure 1b, showing that each of the two middle points can interchange (first tier) and that this interchange can occur simultaneously (second tier). The third and fourth tiers are trivial, as any ordered triple of points can only be simultaneously smoothly deformed to itself along a real loop.

Although real monodromy action was defined in general in [8], the brute force computational approach described in [8, Alg. 1] was limited to $\mathbb{R}^2$. Our main contribution is to formulate real monodromy action in terms of smoothly connected components of real solution sets of fiber product systems [24]. With this formulation, we then utilize an algorithmic approach for computing smoothly connected components via routing functions [3]. This formulation is demonstrated on several real-world leg length and packaging constraints in Section 5.3.

The rest of the paper is structured as follows. Sections 2 and 3 provide an overview of monodromy over the complex and real numbers, respectively. Section 4 describes an algorithm for computing real monodromy action, which is applied to several examples in Section 5. A short conclusion is provided in Section 6.

2 Monodromy over the complex numbers

The following describes the general framework for monodromy groups in $\mathbb{C}$. In particular, let $Y \subset \mathbb{C}^P$ and $U \subset \mathbb{C}^n \times Y$ be irreducible algebraic sets, $f(z,t) : U \to \mathbb{C}^n$ be a polynomial system, $\pi : U \to Y$ be the projection map $\pi(z,t) = t$, and $X \subset U$ be an irreducible component of

$$V_U(f) = U \cap V_{\mathbb{C}}(f) = \{(z,t) \in U \mid f(z,t) = 0\} \subset U$$

such that $\dim X = \dim Y$ and $\overline{\pi(X)} = Y$. Here, the closure of $\pi(X)$ is the same in either the Euclidean or Zariski topology. Hence, there exists $d \geqslant 1$ such that $\pi : X \to Y$ is a d-sheeted branched covering. Thus, for generic $t^* \in Y$, $X \cap \pi^{-1}(t^*)$ consists of d points. If $z_1^*, \ldots, z_d^* \in \mathbb{C}^n$ such that $\{(z_1^*, t^*), \ldots, (z_d^*, t^*)\} = X \cap \pi^{-1}(t^*)$, by utilizing isosingular deflation [11] as needed, we can assume that z_j^* is a nonsingular solution of $f(z, t^*) = 0$, i.e., $\det J_z f(z_j^*, t^*) \neq 0$ where $J_z f(z,t)$ is the Jacobian matrix of f with respect to z evaluated at (z,t). By an abuse of notation, we say that for generic $t^* \in Y$, $f(z,t^*) = 0$ has d nonsingular solutions in $X \cap \pi^{-1}(t^*)$.

There are two sets that we will avoid. First, let $Y_{\text{sing}} = \text{Sing}(Y)$ denote the singular points of Y, which is a proper Zariski closed subset of Y. Second, let $B_d \subset Y$ consist of all $t^* \in Y$ for which $f(z,t^*) = 0$ does not have d nonsingular solutions in $X \cap \pi^{-1}(t^*)$, which is also contained in a proper Zariski closed subset of Y. Hence, we consider $B = Y_{\text{sing}} \cup B_d$ so that π is a d-sheeted covering map from $X \cap \pi^{-1}(Y \backslash B)$ to $Y \backslash B$.

Example 2.1 *Let $Y = \mathbb{C}$, $U = \mathbb{C} \times Y = \mathbb{C}^2$, $f(z,t) = z^3 - t$, $X = V_{\mathbb{C}}(f)$, and $\pi(z,t) = t$. Hence, $\pi : X \to Y$ is a 3-sheeted branched covering that is pictorially illustrated in Figure 1a. Since $Y = \mathbb{C}$, $Y_{\text{sing}} = \varnothing$. Also, $B_3 = \{0\}$ since $z^3 = 0$ has a singular solution while $z^3 - t^* = 0$ has 3 nonsingular solutions for every $t^* \neq 0$. Thus, $B = Y_{\text{sing}} \cup B_3 = \{0\}$ and $X \cap \pi^{-1}(Y \backslash B) = X \backslash \{(0,0)\}$. Therefore, π is a 3-sheeting covering map from $X \backslash \{(0,0)\}$ to $Y \backslash \{0\}$.*

Since π is a d-sheeted covering map from $X \cap \pi^{-1}(Y \backslash B)$ to $Y \backslash B$, the corresponding monodromy group $M_\pi \subset S_d$ is the group of deck transformations of this covering map. In particular, fix a base point $t^* \in Y \backslash B$ and an ordering of the d points in $X \cap \pi^{-1}(t^*)$, say $(z_1^*, t^*), \ldots, (z_d^*, t^*)$. A loop $\ell \subset Y \backslash B$ which starts and ends at t^* lifts to d paths in $X \cap \pi^{-1}(Y \backslash B)$ yielding a permutation $\sigma_\ell \in S_d$ such that the path starting at (z_j^*, t^*) ends at $(z_{\sigma_\ell(j)}^*, t^*)$. Therefore, M_π is the subgroup of S_d

generated by all such permutations σ_ℓ where $\ell \subset Y\backslash B$ is a loop that starts and ends at t^*. In particular, if $\ell_1, \ldots, \ell_k$ is a basis for the fundamental group of $Y\backslash B$ with base point t^*, then

$$M_\pi = \langle \sigma_{\ell_1}, \ldots, \sigma_{\ell_k} \rangle \subset S_d. \tag{3}$$

Since $Y\backslash B$ is connected, M_π is independent of the choice of $t^* \in Y\backslash B$.

Example 2.2 *Continuing with Example 2.1, we can take* $t^* = 1$, $z_1^* = 1$, $z_2^* = \omega$, *and* $z_3^* = \omega^2$ *where* $\omega = e^{2\pi \mathrm{i}/3}$ *is the primitive* 3^{rd} *root of unity. The fundamental group of* $Y\backslash B$ *with base point* t^* *is generated by a single loop, say* $\ell(\tau) = e^{2\pi\tau \mathrm{i}}$ *as* τ *goes from* 0 *to* 1. *Lifting* ℓ *to* $X \cap \pi^{-1}(Y\backslash B)$ *produces* 3 *paths that yield the cyclic permutation* $(1,2,3) \in S_3$ *(using cycle notation for permutations) as illustrated in Figure 1a. Therefore, the monodromy group* M_π *is the cyclic group of order* 3, $\mathbb{Z}_3$, *namely (using cycle notation for permutations)*

$$M_\pi = \langle (1,2,3) \rangle = \{(1,2,3), (1,3,2), (1)\} \subset S_3 \tag{4}$$

where the elements in M_π *are obtained by looping around* ℓ *once, twice, and three times, respectively.*

One can also compute the mondromy group using a fiber product approach (e.g., see [24]) as described in [9, 25]. For $j = 1, \ldots, d$, let

$$F_j(z^{(1)}, \ldots, z^{(j)}, t) = \begin{bmatrix} f(z^{(1)}, t) \\ \vdots \\ f(z^{(j)}, t) \end{bmatrix} \tag{5}$$

be the j^{th} fiber product system defined on $(\mathbb{C}^n)^j \times Y$. Additionally, let

$$\Delta_j = \left\{ (z^{(1)}, \ldots, z^{(j)}, t) \;\middle|\; \text{there exists } 1 \leqslant a < b \leqslant j \text{ with } z^{(a)} = z^{(b)} \right\} \subset (\mathbb{C}^n)^j \times Y$$

be the j^{th} big diagonal where at least two points in different copies of $\mathbb{C}^n$ are equal. Define

$$\pi_j(z^{(1)}, \ldots, z^{(j)}, t) = t \quad \text{and} \quad X_j = \{(z^{(1)}, \ldots, z^{(j)}, t) \mid (z^{(a)}, t) \in X \text{ for } a = 1, \ldots, j\}. \tag{6}$$

The closure of $(X_j \backslash \Delta_j) \cap \pi_j^{-1}(Y\backslash B)$, which is the same in either Euclidean or Zariski topology, has an irreducible decomposition and each irreducible component maps dominantly to Y. In particular, when $j = d$ and $\mathcal{Z}^* = (z_1^*, \ldots, z_d^*, t^*)$, there is a unique irreducible component, say $\mathcal{V}_{\mathcal{Z}^*}$, which contains $\mathcal{Z}^*$ and the mondromy group M_π is computed from $\mathcal{V}_{\mathcal{Z}^*}$ since

$$M_\pi = \left\{ \sigma \in S_d \;\middle|\; \left(z_{\sigma(1)}^*, \ldots, z_{\sigma(d)}^*, t^*\right) \in \mathcal{V}_{\mathcal{Z}^*} \right\}. \tag{7}$$

Example 2.3 *Continuing with Examples 2.1 and 2.2, define* $(\alpha, \beta, \gamma) = \left(z^{(1)}, z^{(2)}, z^{(3)}\right)$ *for ease of presentation so that* F_3 *is the polynomial system*

$$F_3(\alpha, \beta, \gamma, t) = \begin{bmatrix} \alpha^3 - t \\ \beta^3 - t \\ \gamma^3 - t \end{bmatrix}.$$

The set $V_{\mathbb{C}}(F_3)$ *has* 9 *irreducible components of which* 2 *are not contained in* Δ_3. *In particular, the unique irreducible component* $\mathcal{V}_{\mathcal{Z}^*} \subset V_{\mathbb{C}}(F_3)$ *containing* $\mathcal{Z}^* = (1, \omega, \omega^2, 1)$ *is*

$$\mathcal{V}_{\mathcal{Z}^*} = V_{\mathbb{C}}(\alpha + \beta + \gamma, \quad \beta - \omega\alpha, \quad \gamma - \omega\beta, \quad \beta^2 + \beta\gamma + \gamma^2, \quad \gamma^3 - t) \subset \mathbb{C}^4$$

with $\mathcal{V}_{\mathcal{Z}^*} \cap \pi_3^{-1}(1) = \{(1, \omega, \omega^2, 1), (\omega^2, 1, \omega, 1), (\omega, \omega^2, 1, 1)\}$. *Therefore,* (7) *also yields that the monodromy group* M_π *is as listed in* (4).

Example 2.4 *Consider the depressed cubic $f(z,t) = z^3 + t_1 z + t_2$ with $Y = \mathbb{C}^2$, $U = \mathbb{C} \times Y = \mathbb{C}^3$, $X = V_{\mathbb{C}}(f)$, and $\pi(z,t) = t$. For F_3 as in (5), $V_{\mathbb{C}}(F_3)$ has a unique irreducible component not contained in Δ_3 so that $M_\pi = S_3$.*

The approach in (3) for computing the monodromy group utilized a basis of the fundamental group of $Y \backslash B$ and obtained a generating set of permutations in the monodromy group by lifting the loops to solution paths yielding permutations. Conversely, the approach in (7) described the monodromy group by using membership testing of an irreducible component in which its set of smooth points is connected. The key observation is that one is able to repeat a similar approach to (7) with smoothly connected components over the real numbers to compute real monodromy action.

3 Monodromy over the real numbers

In order to mimic the constructions from Section 2 over the real numbers, it is natural to replace irreducible algebraic sets over the complex numbers, whose smooth points are connected, with smoothly connected semialgebraic sets. A basic semialgebraic set $A \subset \mathbb{R}^n$ is a set of the form

$$A = \{x \in \mathbb{R}^n \mid p_1(x) = \cdots = p_e(x) = 0, q_1(x) > 0, \ldots, q_m(x) > 0\} \tag{8}$$

where $e, m \geqslant 0$ such that $p_1, \ldots, p_e, q_1, \ldots, q_m \in \mathbb{R}[x_1, \ldots, x_n]$. If $m = 0$, then A is called a real algebraic set. A semialgebraic set is a finite union of basic semialgebraic sets. A semialgebraic set $A \subset \mathbb{R}^n$ is connected if, for every $\alpha, \beta \in A$, there exists a path $\delta : [0,1] \to A$ with $\delta(0) = \alpha$ and $\delta(1) = \beta$. Let $\overline{A} \subset \mathbb{C}^n$ denote the Zariski closure of A in $\mathbb{C}^n$, which will be the case throughout this section. A connected semialgebraic set $A \subset \mathbb{R}^n$ is smoothly connected if $A \subset \overline{A} \backslash \overline{A}_{\text{sing}}$, i.e., A is contained in the set of smooth points of its Zariski closure. For a semialgebraic set $A \subset \mathbb{R}^n$, the connected components of $\overline{A} \backslash \overline{A}_{\text{sing}} \cap A$ are the smoothly connected components of A.

Example 3.1 *Consider the real points of the Whitney umbrella, namely $A = V_{\mathbb{R}}(x_1^2 - x_2^2 x_3) \subset \mathbb{R}^3$ as illustrated in Figure 3. The real algebraic set A is connected but not smoothly connected due to the "handle," which is the line $V_{\mathbb{R}}(x_1, x_2)$. The smoothly connected components of A are*

$$A_1 = \{x \in \mathbb{R}^3 \mid x_1^2 - x_2^2 x_3 = 0, x_2 < 0\} \quad \text{and} \quad A_2 = \{x \in \mathbb{R}^3 \mid x_1^2 - x_2^2 x_3 = 0, x_2 > 0\}$$

as pictorially represented in Figure 3.

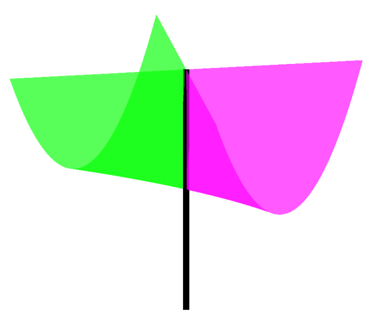

Figure 3: Real points of the Whitney umbrella

Let $Y \subset \mathbb{R}^P$ and $U \subset \mathbb{R}^n \times Y$ be smoothly connected semialgebraic sets, $f(z,t) : U \to \mathbb{R}^n$ be a polynomial system, $\pi : U \to Y$ be the projection map $\pi(z,t) = t$, and $X \subset U$ be a smoothly connected component of

$$V_U(f) = U \cap V_{\mathbb{R}}(f) = \{(z,t) \in U \mid f(z,t) = 0\} \subset U$$

such that $\dim X = \dim Y$ and $\overline{\pi(X)} \cap Y = Y$. For each $d \geqslant 0$, define

$$Y_d = \left\{ t^* \in Y \;\middle|\; \begin{array}{l} \exists \epsilon > 0 \text{ such that, } \forall t \in Y \text{ with } |t - t^*| < \epsilon, \quad X \cap \pi^{-1}(t) \text{ consists} \\ \text{of } d \text{ points which are all nonsingular with respect to } f(z,t) \end{array} \right\}. \tag{9}$$

If $d \geqslant 0$ such that $\overline{Y_d} \cap Y = Y$, then d is called a typical number of solutions. Over the real numbers, there can be more than one typical number of solutions.

Example 3.2 *For the polynomial system G in (2), for generic $(r^*, s^*) \in \mathbb{C}$, $G(x, y, r^*, s^*) = 0$ has 6 nonsingular solutions in $\mathbb{C}^2$. The set $B_6 \subset \mathbb{C}^2$ where this does not hold is*

$$B_6 = V_{\mathbb{C}}(r) \cup V_{\mathbb{C}}(r^2 + s^2) \cup V_{\mathbb{C}}(r^2 s^2 - 4r^2 - 4).$$

In fact, as $r \to 0$, the two solutions satisfying $rx^2 + 1 = 2xy - s = 0$ diverge to infinity. The other two components of B_6 arise from the discriminant locus such that, generically on either $V_{\mathbb{C}}(r^2 + s^2)$ or $V_{\mathbb{C}}(r^2 s^2 - 4r^2 - 4)$, there are 2 nonsingular solutions and 2 solutions of multiplicity 2 in $\mathbb{C}^2$.

Now, we consider the behavior over the real numbers. Note $V_{\mathbb{R}}(r^2 + s^2) = \{(0,0)\} \subset V_{\mathbb{R}}(r)$. For $(r^*, s^*) \in \mathbb{R}^2$, the maximum number of nonsingular real solutions of $G(x, y, r^*, s^*) = 0$ is 4 with a necessary condition being $r^* < 0$. When $(r^*, s^*) \in V_{\mathbb{R}}(r^2 s^2 - 4r^2 - 4)$ with $r^* > 0$, the two singular solutions are non-real so that $G(x, y, r^*, s^*) = 0$ has 2 real nonsingular solutions for all $(r^*, s^*) \in \mathbb{R}^2$ with $r^* > 0$. Conversely, when $(r^*, s^*) \in V_{\mathbb{R}}(r^2 s^2 - 4r^2 - 4)$ with $r^* < 0$, the two singular solutions are real. Figure 2 puts this all together to provide a graphical illustration of the decomposition of $\mathbb{R}^2$ based on the number of real nonsingular solutions of G into 4 smoothly connected components. In particular, for $Y = \mathbb{R}^2$ and $U = \mathbb{R}^2 \times Y = \mathbb{R}^4$, the typical number of solutions is 2 and 4 with

$$Y_4 = \{(r,s) \in \mathbb{R}^2 \mid r < 0, \; r^2 s^2 - 4r^2 - 4 \neq 0\} \quad \textit{and} \quad Y_2 = \{(r,s) \in \mathbb{R}^2 \mid r > 0\} \tag{10}$$

consisting of three and one smoothly connected components, respectively, shown in Figure 2.

Let $d > 0$ be a typical number of solutions, and fix a smoothly connected component of Y_d, say C_d. Since $\pi : X \cap \pi^{-1}(C_d) \to C_d$ is a d-sheeting covering map, one can define the real monodromy group of π with respect to C_d, namely $M_{\pi, C_d} \subset S_d$, exactly as in the complex case – that is, as the group of deck transformations of this covering map. Hence, if the fundamental group of C_d is trivial, then M_{π, C_d} is also trivial [8, Thm. 3.3], i.e., $M_{\pi, C_d} = \langle (1) \rangle$

Example 3.3 *For the polynomial system G in (2), Example 3.2 determined that 2 and 4 were the typical number of solutions with Y_2 being smoothly connected and Y_4 having three smoothly connected components as illustrated in Figure 2. Since the fundamental group of each of these four is trivial, the four corresponding real monodromy groups are also trivial.*

As mentioned in the Introduction, one can view monodromy over the complex numbers as monodromy over the real numbers by treating $\mathbb{C} \cong \mathbb{R}^2$. In this case, there is a unique typical number of solutions, say d, in which Y_d is smoothly connected and it is a tautology that the real monodromy group M_{π, Y_d} is equal to the monodromy group over the complex numbers.

Example 3.4 *Continuing with Example 2.1 with $z = x + \mathrm{i}y$ and $t = r + \mathrm{i}s$ where $x, y, r, s \in \mathbb{R}$,*

$$f(x + \mathrm{i}y, r + \mathrm{i}s) = (x + \mathrm{i}y)^3 - (r + \mathrm{i}s) = (x^3 - 3xy^2 - r) + \mathrm{i}(3x^2y - y^3 - s).$$

Since both the real and imaginary parts must vanish, one obtains $F(x, y, r, s)$ as in (1). In particular, $F(x, y, r^*, s^*) = 0$ has $d = 3$ real nonsingular solutions for every $(r^*, s^*) \in \mathbb{R}^2 \backslash \{(0, 0)\}$ showing that $Y_3 = \mathbb{R}^2 \backslash \{(0, 0)\}$. A simple loop encircling the origin in $\mathbb{R}^2$ yields a cyclic permutation as illustrated in Figure 1a which yields $M_{\pi,Y_3} = \mathbb{Z}_3$ as expected.

One advantage of looking at all real solutions together simultaneously is that one maintains a group structure since loops can be concatenated together. However, maintaining this group structure is often at the expense of having the real monodromy group be trivial and not capturing how subsets of the real solutions could permute. Due to this, the notion of real monodromy action was defined in [8] to consider monodromy action that arises on subsets of the set of real solutions. The following is a modification of [8, Ex. 3.5] that correctly accounts for the singularities.

Example 3.5 *Continuing with Examples 3.2 and 3.3, fix the base point $t^* = (r^*, s^*) = (-1, 0)$, which is a point in the smoothly connected component*

$$C_4 = \{(r, s) \in \mathbb{R}^2 \mid r < 0, \quad r^2s^2 - 4r^2 - 4 < 0\} \subset Y_4 \tag{11}$$

and label the real solutions of $G(x, y, r^*, s^*) = 0$ as

$$z_1^* = (x_1^*, y_1^*) = (0, 1), \quad z_2^* = (x_2^*, y_2^*) = (0, -1), \quad z_3^* = (x_3^*, y_3^*) = (-1, 0), \quad z_4^* = (x_4^*, y_4^*) = (1, 0).$$

For the loop $\ell(\tau) = (-\cos(2\pi\tau), \sin(2\pi\tau)) \subset \mathbb{R}^2$ where τ goes from 0 to 1, the paths starting at solutions 3 and 4 will diverge to infinity, become non-real, diverge to infinity again, and return to being real as illustrated in Figure 1b. Since such a loop does not lift to four real solution paths, this loop is not allowed when considering the real monodromy group. However, if one concentrates only on solutions 1 and 2, this does lift to two real nonsingular solution paths and interchanges solutions 1 and 2 as illustrated in Figure 1b. Hence, one has a nontrivial real monodromy action which permutes solutions 1 and 2 not captured by the real monodromy group.

The following arises from [8] adapted to the context described above.

Definition 3.6 *With the setup described above, let $d > 0$ be a typical number of solutions, C_d be a smoothly connected component of Y_d, and $t^* \in C_d$. Assign an ordering, say $z_1^*, \dots, z_d^*$, to the d nonsingular solutions of $f(z, t^*) = 0$ such that $(z_j^*, t^*) \in X$.*

Let $\mathrm{Pow}(d)$ be the power set of $\{1, \dots, d\}$ and $\mathrm{OPow}(d)$ be the ordered power set of $\{1, \dots, d\}$ consisting of all ordered subsets. For $1 \leqslant k \leqslant d$, let $\mathrm{OPow}_k(d)$ be the elements in $\mathrm{OPow}(d)$ of cardinality k and $\mathrm{IPow}_k(d)$ be the elements in $\mathrm{OPow}_k(d)$ in which the entries are listed in increasing order.

The real monodromy structure associated with π and C_d is the collection

$$\mathcal{G}_{\pi,C_d,\bullet} = \{\mathcal{G}_{\pi,C_d,1}, \dots \mathcal{G}_{\pi,C_d,d}\}$$

where $\mathcal{G}_{\pi,C_d,k} : \mathrm{IPow}_k(d) \to \mathrm{Pow}(\mathrm{OPow}_k(d))$ for $1 \leqslant k \leqslant d$ is defined as follows. For $k = 1, \dots, d$ and $\mathcal{M} = \{m_1, \dots, m_k\} \in \mathrm{IPow}_k(d)$, define $\mathcal{G}_{\pi,C_d,k}(\mathcal{M})$ to be the set consisting of all ordered subsets $\{q_1, \dots, q_k\} \in \mathrm{OPow}_k(d)$ such that there exists a loop $\ell \subset Y$ starting and ending at t^* where the solution path of $f(z, t) = 0$ over ℓ starting at $(z_{m_j}^*, t^*)$ remains in X, is nonsingular with respect to f, and ends at $(z_{q_j}^*, t^*)$ for $j = 1, \dots, k$, i.e., $(z_{m_1}^*, \dots, z_{m_k}^*) \xrightarrow{\ell} (z_{q_1}^*, \dots, z_{q_k}^*)$ using the notation from the Introduction.

The two key differences between the real monodromy group and the real monodromy structure are whether all solutions must be considered simultaneously or not, and where each loop ℓ must live, namely $\ell \subset C_d \subset Y_d \subset Y$ and $\ell \subset Y$, respectively. By taking ℓ to be the trivial loop that remains at t^*, one always has $\mathcal{M} \in \mathcal{G}_{\pi,C_d,k}(\mathcal{M})$. The k^{th} tier $\mathcal{G}_{\pi,C_d,k}$ is said to be trivial if $\mathcal{G}_{\pi,C_d,k}(\mathcal{M}) = \mathcal{M}$ for all $\mathcal{M} \in \text{IPow}_k(d)$. The real monodromy structure $\mathcal{G}_{\pi,C_d,\bullet}$ is trivial if every tier is trivial.

Example 3.7 *Reconsider the depressed cubic $f(z,t) = z^3 + t_1 z + t_2$ from Example 2.4, but now take $Y = \mathbb{R}^2$, $U = \mathbb{R} \times Y = \mathbb{R}^3$, and $\pi(z,t) = t$. Since it is easy to observe that $V_{\mathbb{R}}(f)$ is a graph described by $(z,t_1) \mapsto (z, t_1, -z^3 - t_1 z)$, $V_{\mathbb{R}}(f)$ is smooth and connected so we take $X = V_{\mathbb{R}}(f)$. It is classically known that 1 and 3 are the typical number of solutions with*

$$Y_1 = \{(t_1,t_2) \in \mathbb{R}^2 \mid 4t_1^3 + 27t_2^2 > 0\} \quad \textit{and} \quad Y_3 = \{(t_1,t_2) \in \mathbb{R}^2 \mid 4t_1^3 + 27t_2^2 < 0\},$$

which are both connected with each having a trivial fundamental group.

For $d = 1$, we take $C_1 = Y_1$ and fix $t^* = (1,0) \in C_1$. Set $z_1^* = 0$ to be the unique real solution of $f(z,t^*) = z^3 + z = 0$. Of course, with only one real solution, the real monodromy structure $\mathcal{G}_{\pi,Y_1,\bullet} = \{\mathcal{G}_{\pi,Y_1,1}\}$ is trivial with $\mathcal{G}_{\pi,Y_1,1}(\{1\}) = \{\{1\}\}$.

For something nontrivial, consider $d = 3$ with $C_3 = Y_3$ and $t^* = (-1,0) \in C_3$. Let $z_1^* = 1$, $z_2^* = 0$, and $z_3^* = -1$ be the three real solutions of $f(z,t^*) = z^3 - z = 0$. For the loop $\ell \subset \mathbb{R}^2$ defined by $(-cos(\theta), \sin(\theta))$ for θ from 0 to 2π which starts and ends at t^*, the solution path over ℓ starting at (z_1^*, t^*) ends at (z_3^*, t^*) is illustrated in Figure 4. From this picture, one can also observe that, for any loop $\delta \subset \mathbb{R}^2$ with starts and ends at t^*, the solution paths over δ starting at (z_2^*, t^*) remains nonsingular if and only if $\delta \subset Y_3$, which is contractible since the fundamental group of Y_3 is trivial. Hence, such a path must also end at (z_2^*, t^*). Therefore, $\mathcal{G}_{\pi,Y_3,1}$ is as follows:

- $\{1\}$, $\{3\} \mapsto \{\{1\},\{3\}\}$
- $\{2\} \mapsto \{\{2\}\}$.

It follows from the analysis of the first tier that the only potentially possible nontrivial part of the second tier $\mathcal{G}_{\pi,Y_3,2}$ could be a simultaneous smooth interchange of (z_1^*, t^*) and (z_3^*, t^*) over the

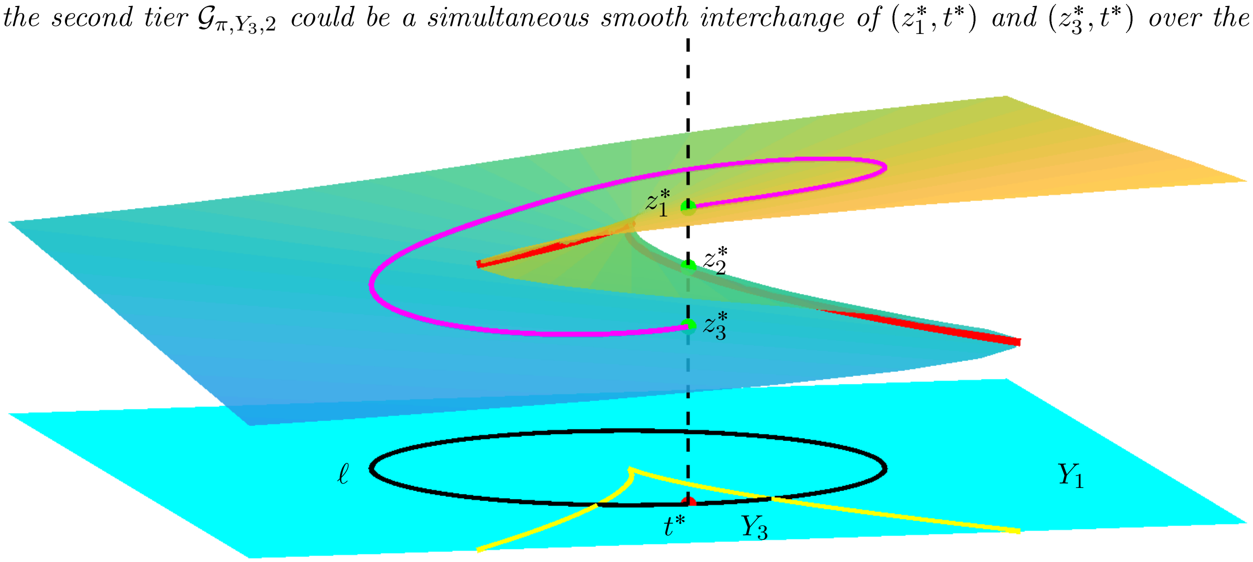

Figure 4: Illustrating real monodromy action for the depressed cubic

real numbers. However, this cannot happen since the fundamental group of Y_3 is trivial implies that this loop would need to leave Y_3 and enter Y_1 where two real paths cannot exist simultaneously. Hence, $\mathcal{G}_{\pi,Y_3,2}$ is trivial. By similar reasoning, $\mathcal{G}_{\pi,Y_3,3}$ is also trivial.

Note that the monodromy group over the complex numbers computed in Example 2.4 is S_3, showing that all three solutions can be permuted freely over the complex numbers. However, over the real numbers, the real monodromy structure has only one nontrivial action which arises in the first tier associated with only two of three real solutions, namely z_1^* and z_3^*.

Example 3.8 *Continuing with Examples 3.2 and 3.3, there are four different real monodromy structures that arise and each is described below.*

For C_4 in (11), taking $t^* = (r^*, s^*) = (-1, 0) \in C_4$ together with the ordering in Example 3.5, solutions 1 and 2 can interchange as illustrated in Figure 1b. Since solutions 3 and 4 become singular along the boundary $r^2s^2 - 4r^2 - 4 = 0$ and diverge to infinity at $r = 0$, the real monodromy structure associated with solutions 3 and 4 is trivial so $\mathcal{G}_{\pi,C_4,\bullet} = \{\mathcal{G}_{\pi,C_4,1}, \mathcal{G}_{\pi,C_4,2}, \mathcal{G}_{\pi,C_4,3}, \mathcal{G}_{\pi,C_4,4}\}$ is as follows:

- $\mathcal{G}_{\pi,C_4,1}$:
  - $\{1\}, \{2\} \mapsto \{\{1\}, \{2\}\}$
  - $\{m_1\} \mapsto \{\{m_1\}\}$ *for all others*
- $\mathcal{G}_{\pi,C_4,2}$:
  - $\{1, 2\} \mapsto \{\{1, 2\}, \{2, 1\}\}$
  - $\{m_1, m_2\} \mapsto \{\{m_1, m_2\}\}$ *for all others.*

with trivial $\mathcal{G}_{\pi,C_4,3}$ and $\mathcal{G}_{\pi,C_4,4}$. In fact, the corresponding real monodromy group M_{π,C_4}, which consider all real solutions simultaneously, is trivial.

The real monodromy structures for the other two connected components of Y_4 are trivial since all four real solutions become singular on the boundary $r^2s^2 - 4r^2 - 4 = 0$ and the fundamental group of each smoothly connected component is trivial.

Finally, consider Y_2 as in (10), which is smoothly connected, and $t^* = (r^*, s^*) = (1, 0) \in Y_2$. With the labeling $z_1^* = (1, 0)$ and $z_2^* = (-1, 0)$, the loop $\ell(\tau) = (\cos(2\pi\tau), \sin(2\pi\tau))$ where τ goes from 0 to 1 interchanges the points as observed in Figure 1b. Thus, the real monodromy structure $\mathcal{G}_{\pi,Y_2,\bullet} = \{\mathcal{G}_{\pi,Y_2,1}, \mathcal{G}_{\pi,Y_2,2}\}$ is as follows:

- $\mathcal{G}_{\pi,Y_2,1}$:
  - $\{1\}, \{2\} \mapsto \{\{1\}, \{2\}\}$
- $\mathcal{G}_{\pi,Y_2,2}$:
  - $\{1, 2\} \mapsto \{\{1, 2\}, \{2, 1\}\}$.

This has the structure of the group S_2 as the two points can be interchanged simultaneously. Conversely, the corresponding real monodromy group M_{π,Y_2} is trivial since the fundamental group of Y_2 is trivial. The reason for this difference is that the loop to interchange the two solutions leaves Y_2 so that the number of real solutions is not constant along the loop, but these extra solutions that appear and disappear along the loop have no impact on the lifted solution paths. Therefore, this interchange of real solutions is captured by the real monodromy structure but not the real monodromy group.

The following considers real monodromy action over sets which are not affine.

Example 3.9 *For $z = (x, y) \in \mathbb{R}^2$ and $t \in \mathbb{R}^3$, consider the polynomial system*

$$f(z,t) = \begin{bmatrix} x^2 - y^2 - 2t_1 + 3 \\ 2xy - t_3 \end{bmatrix}.$$

First, consider $Y = \mathbb{T} \subset \mathbb{R}^3$ to be the torus

$$\mathbb{T} = \{(t_1, t_2, t_3) \in \mathbb{R}^3 \mid (t_1^2 + t_2^2 + t_3^2 + 3)^2 - 16(t_1^2 + t_2^2) = 0\}$$

and $f : U \to \mathbb{R}^2$ where $U = \mathbb{R}^2 \times \mathbb{T}$. For all $t \in \mathbb{T} \backslash V_{\mathbb{R}}(2t_1 - 3, t_3) = \mathbb{T} \backslash \{(3/2, \pm 3/2\sqrt{3}, 0)\}$ as illustrated in Figure 5a, $f(z,t) = 0$ has two nonsingular real solutions. Hence, $d = 2$ is the typical number of solutions and $Y_2 = \mathbb{T} \backslash \{(3/2, \pm 3/2\sqrt{3}, 0)\}$. Since encircling either of the removed points interchanges the two real solutions, the real monodromy structure for Y_2 corresponds precisely with the real monodromy group, namely S_2.

Now, if we take $U = \{(z_1, z_2) \in \mathbb{R}^2 \mid z_1^2 + z_2^2 > 2\} \times \mathbb{T}$, then $d = 2$ is still the typical number of solutions, but Y_2 has two smoothly connected components as illustrated in Figure 5b. With this change, the real monodromy structure and real monodromy group associated with both smoothly connected components become trivial.

The final item for this section is our main theoretical result regarding the relationship between fiber products and real monodromy structure.

Theorem 3.10 *With the setup described above, suppose that $d > 0$ such that d is a typical number of solutions and $t^* \in C_d \subset Y_d$ where C_d is a smoothly connected component of Y_d. Assign an ordering, say $z_1^*, \ldots, z_d^*$, to the d nonsingular solutions of $f(z, t^*) = 0$ such that $(z_j^*, t^*) \in X$. Fix $j \in \{1, \ldots, d\}$ and let F_j and X_j be as in (5) and (6), respectively. For each $1 \leqslant k_1 < \cdots < k_j \leqslant d$ with $\mathcal{Z}^* = (z_{k_1}^*, \ldots, z_{k_j}^*, t^*)$, there exists a unique smoothly connected component $\mathcal{V}_{j,\mathcal{Z}^*}$ of $V_{X_j}(F_j)$ that contains $\mathcal{Z}^*$. Moreover, for $o = \{o_1, \ldots, o_j\} \in \mathrm{OPow}_j(d)$, then $o \in \mathcal{G}_{\pi, C_d, j}(\{k_1, \ldots, k_j\})$ if and only if $(z_{o_1}^*, \ldots, z_{o_j}^*, t^*) \in \mathcal{V}_{j,\mathcal{Z}^*}$.*

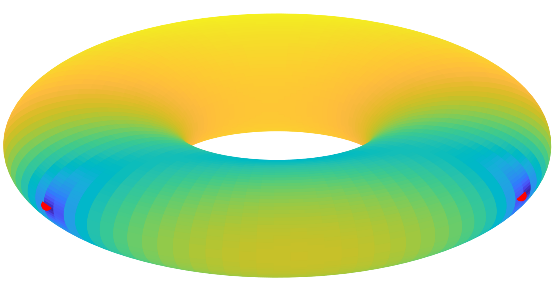

(a)

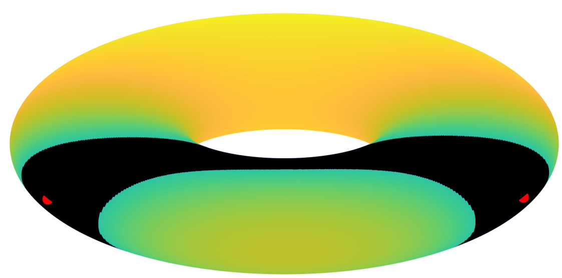

(b)

Figure 5: (a) Illustrating $t \in \mathbb{T}$ with the color based on the Euclidean distance between the two real solutions of $f(z,t) = 0$ with the points $(3/2, \pm 3/2\sqrt{3}, 0)$ marked. (b) Illustrating $t \in \mathbb{T}$ such that there is a real solution of $f(z,t) = 0$ with $x^2 + y^2 > 2$ where the color is based on the Euclidean distance between the two real solutions of $f(z,t) = 0$ with the points $(3/2, \pm 3/2\sqrt{3}, 0)$ marked.

Proof. The assumptions yield that $\mathcal{Z}^* = (z_{k_1}^*, \ldots, z_{k_j}^*, t^*)$ must be a smooth point on the set $(V_{X_j}(F_j)\backslash\Delta_j) \cap \pi^{-1}(U\backslash B)$. Hence, there exists a unique smoothly connected component, $\mathcal{V}_{j,\mathcal{Z}^*}$, of this set which contains $\mathcal{Z}^*$. If $o \in \mathrm{OPow}_j(d)$ with $o \in \mathcal{G}_{\pi,C_d,j}(\{k_1,\ldots,k_j\})$, then Definition 3.6 provides that $(z_{k_1}^*, \ldots, z_{k_j}^*, t^*)$ and $(z_{o_1}^*, \ldots, z_{o_j}^*, t^*)$ must both lie in $\mathcal{V}_{j,\mathcal{Z}^*}$. Similarly, if $o \in \mathrm{OPow}_j(d)$ with $(z_{o_1}^*, \ldots, z_{o_j}^*, t^*) \in \mathcal{V}_{j,\mathcal{Z}^*}$, then there is a smooth path in $\mathcal{V}_{j,\mathcal{Z}^*}$ connecting $(z_{k_1}^*, \ldots, z_{k_j}^*, t^*)$ and $(z_{o_1}^*, \ldots, z_{o_j}^*, t^*)$. Letting ℓ be the projection under π_j as in (6) of this smooth path in $\mathcal{V}_{j,\mathcal{Z}^*}$, then $\ell \subset Y$ is a loop starting and ending at t^* such that Definition 3.6 yields $o \in \mathcal{G}_{\pi,C_d,j}(\{k_1,\ldots,k_j\})$. □

Theorem 3.10 immediately yields an algorithm for computing real monodromy structures which is described in detail in the next section after closing out this section with two examples.

Example 3.11 *To illustrate Theorem 3.10, consider $Y = \mathbb{R}^2$, $U = \mathbb{R}^2 \times Y = \mathbb{R}^4$, $\pi(x,y,t) = t$,*

$$f(x,y,t) = \begin{bmatrix} x^2 - y^2 - t_1 \\ 2xy - t_2 \end{bmatrix} = 0.$$

Since $f(x,y,t) = 0$ defines a graph, it easy to observe that $X = V_{\mathbb{R}}(f) \subset \mathbb{R}^4$ is smoothly connected and π is a 2-sheeted covering map from $X\backslash\{(0,0,0,0)\}$ to $Y_2 = \mathbb{R}^2\backslash\{(0,0)\}$ where $d = 2$ is the typical number of solutions. Since Y_2 is smoothly connected, $C_2 = Y_2$, and thus there is one real monodromy structure that we aim to compute, namely $\mathcal{G}_{\pi,Y_2,\bullet}$. Fix $t^* = (1,0)$ and label the two real solutions as $z_1^* = (1,0)$, and $z_2^* = (-1,0)$.

$j = 1$: For $\mathcal{Z}^* = (z_1^*, t^*)$, since $X_1 = X$ is smoothly connected, $\mathcal{V}_{1,\mathcal{Z}^*} = X$ with $\mathcal{Z}^*$ and (z_2^*, t^*) are both contained in $\mathcal{V}_{1,p^*}$ so that $\mathcal{G}_1(\{1\}) = \mathcal{G}_1(\{2\}) = \{\{1\},\{2\}\}$.

$j = 2$: For $\mathcal{Z}^* = (z_1^*, z_2^*, t^*)$, outside of Δ_2, there is one smoothly connected component of X_2, namely $\mathcal{V}_{2,\mathcal{Z}^*}$ which contains both $\mathcal{Z}^*$ and (z_2^*, z_1^*, t^*). Hence, this shows $\mathcal{G}_2(\{1,2\}) = \{\{1,2\},\{2,1\}\}$.

The tiers of $\mathcal{G}_{\pi,Y_2,\bullet}$ are all as expected since $f(z,t)$ arises from $\mathbb{C} \cong \mathbb{R}^2$ applied to $\zeta^2 - \tau = 0$ which has monodromy group S_2. Hence, the corresponding real monodromy group is S_2 and the real monodromy structure encodes S_2.

Example 3.12 *Continuing with Examples 3.2 and 3.3, there are 11 smoothly connected components of $V_U(G)$. A summary of these 11 in relation to the real monodromy structure is described in Example 3.8 is as follows.*

Three smoothly connected components are illustrated in Figure 1b with two of them arising over the middle left connected component of Figure 2, each associated with a real solution. The other lies over the middle left and right connected component illustrated in Figure 2 associated with two real solutions over both connected components. This structure is captured in $\mathcal{G}_{\pi,C_4,\bullet}$ and $\mathcal{G}_{\pi,Y_2,\bullet}$ presented in Example 3.8.

Over both the upper and lower left connected components of Figure 2, there are four smoothly connected components, one for each of the four real solutions. This accounts for the other eight smoothly connected components and is in agreement with both having trivial real monodromy structures as described in Example 3.8.

4 Algorithm for computing real monodromy action

Theorem 3.10 shows that real monodromy action can be determined by performing membership tests with smoothly connected components. By using routing functions summarized in Section 4.1, Section 4.2 provides an algorithm for computing real monodromy action arising from smoothly connected components of basic semialgebraic sets.

4.1 Smooth connectivity and membership testing using routing functions

Homotopy continuation in numerical algebraic geometry (see the books [2,23] for a general overview) provides an approach to compute all isolated solutions to a polynomial system over the complex numbers. Thus, all that remains to turn Theorem 3.10 into an algorithm is to perform membership testing for smoothly connected components. To this end, routing functions, see [3, 13, 14], provide a way of performing membership tests on smoothly connected components of basic semialgebraic sets. The underlying idea is to construct an atlas of routing road maps, one for each smoothly connected component. This is done by computing the critical points of the routing function and then connecting them by routing roads, which are gradient flows of the routing function emanating from the unstable critical points. The membership of a test point is established by following a gradient flow from it. The flow must end at a known routing point, and the road map that contains that routing point identifies which component the test point belongs to.

Suppose that $A \subset \mathbb{R}^n$ is a basic semialgebraic set as in (8) and a polynomial $h \in \mathbb{R}[x_1, \ldots, x_n]$ such that $A \backslash V_{\mathbb{R}}(h)$ is smooth of codimension e. Hence, we aim to compute the connected components of $A \backslash V_{\mathbb{R}}(h)$. Let $b = h \cdot q_1 \cdots q_m$, $c \in \mathbb{R}^n$, and $\kappa \in \mathbb{Z}_{>0}$ such that $2\kappa > \deg(b)$. Define

$$r(x) = \frac{b(x)}{(1 + (x_1 - c_1)^2 + \cdots + (x_n - c_n)^2)^{\kappa}}. \tag{12}$$

For general $c \in \mathbb{R}^n$, r is a routing function on A (see [3, Thm. 3.4] for more details) which, in particular, means that r is a Morse function on $A \backslash V_{\mathbb{R}}(h)$. That is, for general $c \in \mathbb{R}^n$, there are at most finitely many critical points of r on $A \backslash V_{\mathbb{R}}(h)$, called routing points, and each is nondegenerate with the Hessian of r on A evaluated at a critical point having distinct eigenvalues that are all nonzero. One can, for example, compute routing points by using homotopy continuation to solve a polynomial system that enforces criticality using Lagrange multipliers.

Example 4.1 *Reconsider the depressed cubic from Examples 2.4 and 3.7 with $f(z, t) = z^3 + t_1 z + t_2$. Since $U = \mathbb{R}^3$ and $\pi(z, t) = t$, we want to compute the connected components of $V_{\mathbb{R}}(f) \backslash V_{\mathbb{R}}(h)$ where*

$$h = \det J_z f = 3z^2 + t_1$$

yielding a routing function of the form

$$r(z, t) = \frac{b(z, t)}{w(z, t)^{\kappa}} = \frac{3z^2 + t_1}{(1 + (z - c_1)^2 + (t_1 - c_2)^2 + (t_2 - c_3)^2)^{\kappa}}. \tag{13}$$

We may take $\kappa = 2$ and use constants $c_1 = 4/7$, $c_2 = 1/3$, and $c_3 = -2/5$, which are sufficiently general. A point $a \in \mathbb{R}^3 \backslash V_{\mathbb{R}}(h)$ is a routing point if there exists $\lambda \in \mathbb{R}$ such that

$$f(a) = 0, \qquad w(a) \cdot \nabla b(a) - \kappa \cdot b(a) \cdot \nabla w(a) + \lambda \cdot \nabla f(a) = 0 \tag{14}$$

where $\nabla \Phi$ is the gradient of Φ with respect to (z, t_1, t_2). Equations (14) consist of four polynomial equations in $\mathbb{C}^4$, which can be solved using homotopy continuation to find all solutions in $\mathbb{C}^4 \backslash V_{\mathbb{C}}(b, w)$. This yields 12 points in $\mathbb{C}^4 \backslash V_{\mathbb{C}}(b, w)$ of which 2 are real. Hence, rounding to four decimal places, the 2 routing points are $\rho_1 = (0.0456, -0.6155, 0.0280)$ and $\rho_2 = (0.7408, 0.3018, -0.6301)$.

Each routing point has an index which is equal to the number of eigenvalues of the Hessian of r on A with the same sign as r evaluated at the routing point. The eigenvectors corresponding to each such eigenvector are called unstable eigenvectors. In particular, a routing point with index 0 is either a local maximum when $r > 0$ or a local minimum when $r < 0$. The use of κ in the denominator of (12) ensures that every smoothly connected component contains at least one routing point of index 0.

Example 4.2 *The two routing points in Example 4.1 are both index* 0 *with* $r(\rho_1) > 0$ *and* $r(\rho_2) < 0$*. Hence,* ρ_1 *is a local maximum of* r *on* $V_{\mathbb{R}}(f)$ *while* ρ_2 *is a local minimum of* r *on* $V_{\mathbb{R}}(f)$

With the routing points and indices computed, a routing road map is constructed by using gradient flows emanating along the unstable eigenvector directions at the routing points with positive index. Suppose that a is a routing point, v is an unstable eigenvector, and $\nabla_A r$ denotes the gradient of r on A. For every $\epsilon > 0$, the solution $y_\epsilon(s)$ to

$$\begin{array}{rcl} \dot{y}(s) & = & \operatorname{sign}(r(a)) \cdot \nabla_A r(y(s)) \\ y(0) & = & a + \epsilon \cdot v \end{array} \tag{15}$$

is well-defined and

$$\lim_{\epsilon \to 0^+} \lim_{s \to \infty} y_\epsilon(s)$$

is a routing point, called the destination of the gradient flow of r starting at a in the direction v. This destination lies the same smoothly connected component as a. Note that one may obtain different destinations for directions v and $-v$ so one must consider both separately. Looping over routing points and corresponding unstable eigenvector directions v and $-v$ yields a collection of gradient flows that yield a routing road map in which the smoothly connected components are in one-to-one correspondence with the connected components of the road map [3]. The Euler characteristic of a smoothly connected component is equal to the number of routing points on that component with even index minus the number of routing points on that component with odd index.

Example 4.3 *Since Example 4.2 posits that both routing points have index* 0*, the routing road map just consists of two points, namely* ρ_1 *and* ρ_2*. Hence,* $V_{\mathbb{R}}(f)\backslash V_{\mathbb{R}}(h)$ *consists of two connected components, which could be observed by considering Figure 4, each with Euler characteristic of* 1*.*

Finally, given a point $x \in A\backslash V_{\mathbb{R}}(h)$, the last item is to determine which smoothly connected component x belongs to. If x is a routing point, then this is determined directly from the routing road map. When x is not a routing point, then the gradient flow defined by

$$\begin{array}{rcl} \dot{y}(s) & = & \operatorname{sign}(r(x)) \cdot \nabla_A r(y(s)) \\ y(0) & = & x \end{array} \tag{16}$$

must limit to a routing point as $s \to \infty$, called the destination of the gradient flow of r starting at x. The point x and its destination are on the same smoothly connected component which is described via the routing road map.

Example 4.4 *For the depressed cubic* $f(z,t) = z^3 + t_1 z + t_2$ *and routing function* r *in (14) considered in Examples 4.1–4.3, gradient flow is used to determine membership for* (z_j^*, t^*) *for* $j = 1, 2, 3$ *as in Example 3.7 and illustrated in Figure 6. In particular, gradient flow emanating from* (z_1^*, t^*) *and* (z_3^*, t^*) *both end at* ρ_1 *while gradient flow from* (z_2^*, t^*) *ends at* ρ_2*. Hence,* (z_1^*, t^*) *and* (z_3^*, t^*) *are on the same smoothly connected component while* (z_2^*, t^*) *is on a different component.*

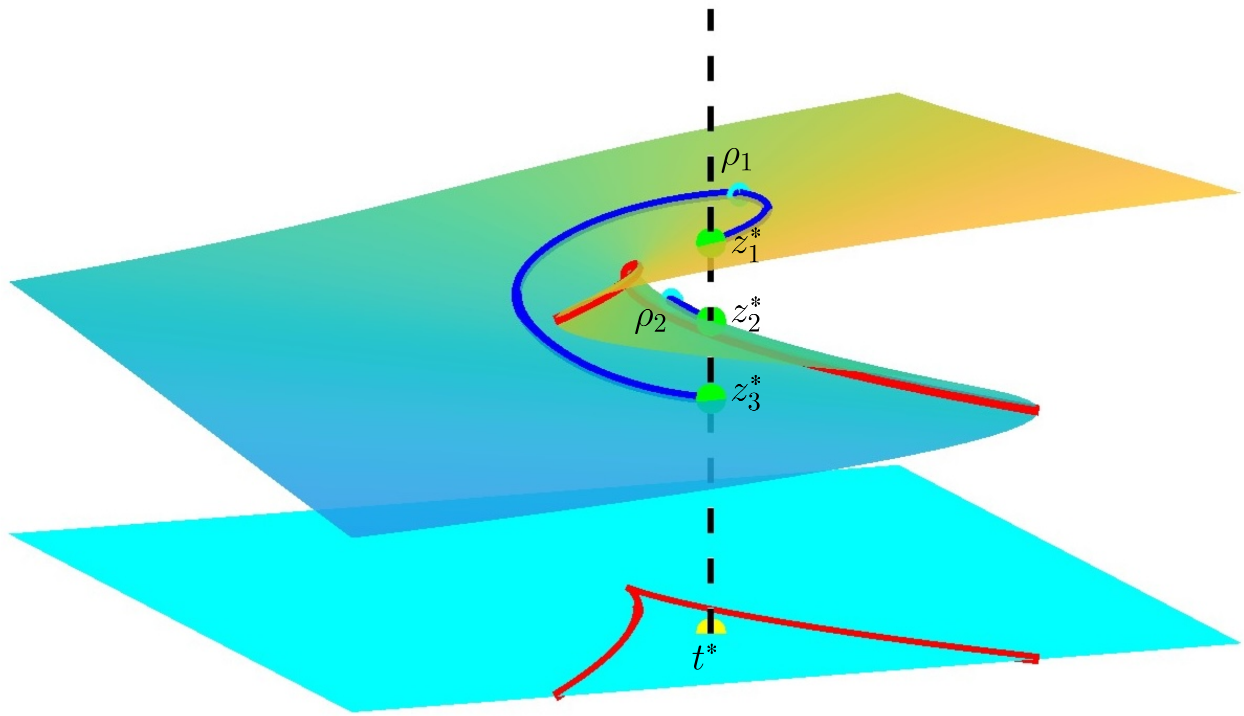

Figure 6: Illustrating membership testing using gradient flow for the depressed cubic.

4.2 Algorithms

Three algorithms are summarized: the first two are preparatory, computing a routing road map and membership testing for smoothly connected components, with the third for computing real monodromy action. The first two algorithms are justified by [3, Thm. 4.4] with Algorithm 1 depending upon a random choice being generic so it holds with probability one. The third algorithm follows from Theorem 3.10. Note that Y_d and the smoothly connected component $C_d \subset Y_d$ such that $t^* \subset C_d \subset Y_d$ are not explicitly computed in Algorithm 3 as they are not needed for determining $\mathcal{G}_{\pi,C_d,j}$. That is, only the given point $t^* \in C_d \subset Y_d$ together with membership testing is sufficient for computing real monodromy action.

For Algorithm 3, Line 1 typically requires the largest computational effort as this requires computing all of the routing points. The loop starting at Line 2 is "embarrassingly parallel" as membership testing can be performed independently. The loop starting at Line 5 is just bookkeeping after all of the membership tests are performed.

5 Examples

The following considers computing real monodromy action for three different polynomial systems: a maximum likelihood estimation problem in algebraic statistics (Section 5.1), steady-states of the Kuramoto model for $n = 3$ and $n = 4$ (Section 5.2), and various types of practical leg length and packaging constraints for a 3RPR linkage (Section 5.3). Routing points were computed using `Bertini` [1] with road map computations and membership testing performed using `MATLAB`.

Algorithm 1 Routing road map

Input: Polynomials $p_1, \ldots, p_e, q_1, \ldots, q_m \in \mathbb{R}[x_1, \ldots, x_n]$ which define a basic semialgebraic set $A \subset \mathbb{R}^n$ as in (8) and a polynomial $h \in \mathbb{R}[x_1, \ldots, x_n]$ such that $A \backslash V_{\mathbb{R}}(h)$ is smooth of codimension e.

Output: Routing function r and a partitioned subset of routing points corresponding to the connected components of $A \backslash V_{\mathbb{R}}(h)$.

```
Select c ∈ ℝ^n randomly, set b = h · q_1 ··· q_m, and κ = ⌈(deg(b) + 1)/2⌉.
Construct r as in (12).
Compute the routing points of r on A and assign an ordering, say ρ_1, ..., ρ_k.
Initialize M = I_k, the k × k identity matrix.
for j = 1, ..., k do
    for each unstable eigenvector v do
        Compute the destination ρ_{v+} of the gradient flow of r starting at ρ_j in the direction v
and set M_{j,v+} = M_{v+,j} = 1.
        Compute the destination ρ_{v−} of the gradient flow of r starting at ρ_j in the direction −v
and set M_{j,v−} = M_{v−,j} = 1.
    end for
end for
Replace matrix M by its transitive closure.
Partition the set {ρ_1, ..., ρ_k} based on the connected components of M, say C_1, ..., C_u.
return r and C_1, ..., C_u
```

Algorithm 2 Membership testing

Input: Polynomials $p_1, \ldots, p_e, q_1, \ldots, q_m \in \mathbb{R}[x_1, \ldots, x_n]$ which define a basic semialgebraic set $A \subset \mathbb{R}^n$ as in (8), a polynomial $h \in \mathbb{R}[x_1, \ldots, x_n]$ such that $A \backslash V_{\mathbb{R}}(h)$ is smooth of codimension e, a routing function r for $A \backslash V_{\mathbb{R}}(h)$, a partitioned subset of routing points $\mathcal{C}_1, \ldots, \mathcal{C}_u$ corresponding to the connected components of $A \backslash V_{\mathbb{R}}(h)$, and a point $x \in A \backslash V_{\mathbb{R}}(h)$

Output: Index $j \in \{1, \ldots, u\}$ such that x and the routing points in $\mathcal{C}_j$ belong to the same connected component of $A \backslash V_{\mathbb{R}}(h)$.

```
if x ∈ C_1 ∪ ··· ∪ C_u then
    Determine the unique j ∈ {1, ..., u} such that x ∈ C_j and return j.
else
    Determine the unique j ∈ {1, ..., u} such that the destination of the gradient of r starting
at x is contained in C_j and return j.
end if
```

5.1 Maximum likelihood

Maximum likelihood estimation (MLE) aims to determine parameters of a probabilistic model that maximize a likelihood function based on observed data. Monodromy describes how the critical points of the likelihood function on the model can permute as the observed data is changed. As a concrete example, we consider a modification of the problem considered in [9, § 5.3] and [21, Ex. 6]

Algorithm 3 Real monodromy action

Input: Routing road map for $Y \subset \mathbb{R}^P$ and $U \subset \mathbb{R}^n \times Y$ which are both a smoothly connected component of a basic semialgebraic set, polynomial system $f : U \to \mathbb{R}^n$, projection map $\pi : U \to Y$, routing road map for $X \subset U$ which is a smoothly connected component of $V_U(f)$ such that $\dim X = \dim Y$ and $\overline{\pi(X)} \cap Y = Y$, $d > 0$, $t^* \in Y_d$ in which $t^* \subset C_d$ where C_d is a smoothly connected component of Y_d, ordering $z_1^*, \ldots, z_d^*$ of the d nonsingular solutions of $f(z, t^*) = 0$ such that $(z_j^*, t^*) \in X$, and $j \in \{1, \ldots, d\}$.

Output: The j^{th} tier of the corresponding real monodromy structure $\mathcal{G}_{\pi,C_d,j}$.

Use Algorithms 1 and Algorithm 2 to compute a routing road map for the smoothly connected components of $V_{X_j}(F_j)$ where F_j and X_j are as in (5) and (6), respectively, with $h = \det J_z f(z_1, t) \cdots \det J_z f(z_j, t)$. This returns, say, the routing function r and partitioned subsets of routing points $\mathcal{C}_1, \ldots, \mathcal{C}_u$.

for $o = \{o_1, \ldots, o_j\} \in \mathrm{OPow}_j(d)$ **do**

    Use Algorithm 2 with r and $\mathcal{C}_1, \ldots, \mathcal{C}_u$ to determine $i_o \in \{1, \ldots, u\}$ such that $(z_{o_1}^*, \ldots, z_{o_j}^*, t^*)$ and the routing points in $\mathcal{C}_{i_o}$ belong to the same smoothly connected component of $V_{X_j}(F_j)$.

end for

for $1 \leqslant k_1 < \cdots < k_j \leqslant d$ **do**

    Set $\mathcal{G}_{\pi,C_d,j}(\{k_1, \ldots, k_j\}) = \{o \in \mathrm{OPow}_j(d) \mid i_{\{k_1,\ldots,k_j\}} = i_o\}$.

end for

return $\mathcal{G}_{\pi,C_d,j}$

constructed as follows. The set of $x \in \mathbb{C}^3$ where the matrix

$$\begin{bmatrix} 2x_1 & x_2 & x_3 \\ x_2 & 2x_1 & x_2 \\ x_3 & x_2 & 2x_1 \end{bmatrix}$$

has rank at most 2 is the union of a plane defined by $x_3 = 2x_1$ and a quadric surface $V_{\mathbb{C}}(p_1)$ where $p_1(x) = 2x_1^2 - x_2^2 + x_1x_3$. For parameters $u = (u_1, u_2, u_3)$ representing observed data, we consider the critical points of the likelihood function $L(u) = x_1^{u_1}x_2^{u_2}x_3^{u_3}$ over $V_{\mathbb{C}}(p_1, p_2)$ where $p_2(x) = x_1 + x_2 + x_3 - 1$. Letting ∇ denote the gradient operator and $\star$ denote the Hadamard (entrywise) product, the critical points satisfy the so-called likelihood equations, namely

$$f(x, \lambda, u) = \begin{bmatrix} p_1(x) \\ p_2(x) \\ x \star (\lambda_1 \nabla p_1(x) + \lambda_2 \nabla p_2(x)) - u \end{bmatrix} = \begin{bmatrix} x_1 + x_2 + x_3 - 1 \\ 2x_1^2 - x_2^2 + x_1x_3 \\ x_1(\lambda_1 + (4x_1 + x_3)\lambda_2) - u_1 \\ x_2(\lambda_1 - 2x_2\lambda_2) - u_2 \\ x_3(\lambda_1 + x_1\lambda_2) - u_3 \end{bmatrix} = 0.$$

The number of solutions to $f(x, \lambda, u^*) = 0$ for generic $u^* \in \mathbb{C}^3$ is called the ML degree which, in this case, is 4. For concreteness, fix $u^* = (20, 3, 4)$ and label the four solutions (rounded to four decimal places) in $z = (x, \lambda)$ coordinates as

$$\begin{aligned} z_1^* &= (\ \ 0.3489,\ 0.5334,\ 0.1177,\ 27,\ 20.0368), & z_2^* &= (-2.0616,\ 2.8338,\ 0.2277,\ 27,\ \ \ 4.5771), \\ z_3^* &= (-0.8221,\ 0.2603,\ 1.5619,\ 27,\ 29.7263), & z_4^* &= (-0.8578,\ 0.1799,\ 1.6779,\ 27,\ 28.6962). \end{aligned}$$

Note that z_1^* is the only solution over u^* with all entries positive so that is corresponds with probabilities in the statistical model. Thus, we aim to determine the monodromy action of this solution as the data u is changed first over the complex numbers and then over the real numbers.

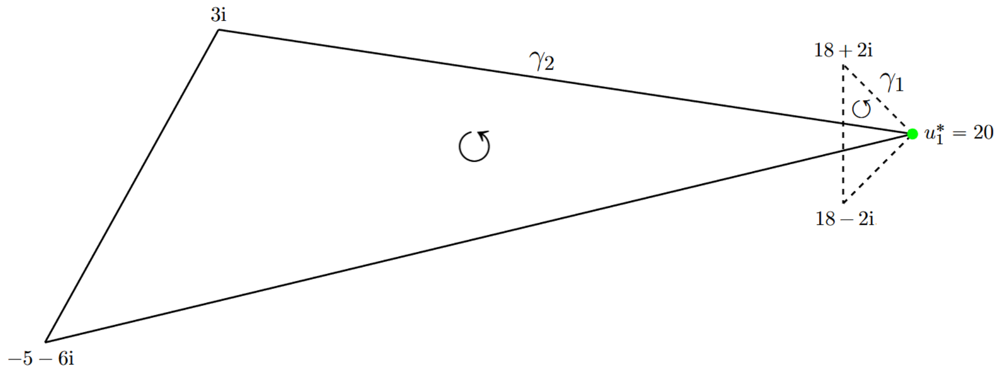

Figure 7: Illustrating loops γ_1 and γ_2

Let $Y = \mathbb{C}^3$, $U = \mathbb{C}^5 \times Y = \mathbb{C}^8$, and $X = V_{\mathbb{C}}(f)$, whose irreducibility immediately follows from the irreducibility of $V_{\mathbb{C}}(p_1, p_2)$. For the projection map $\pi(x, \lambda, u) = u$, we consider the monodromy group $M_\pi \subset S_4$ over the complex numbers. To see that $M_\pi = S_4$, it is enough to show that M_π contains a transposition and a 4-cycle. To that end, we can keep $u_2^* = 3$ and $u_3^* = 4$ fixed and consider triangular loops $\gamma_1 \subset \mathbb{C}$ having vertices $u_1^* = 20$, $18 + 2\mathrm{i}$, and $18 - 2\mathrm{i}$, and $\gamma_2 \subset \mathbb{C}$ having vertices $u_1^* = 20$, $3\mathrm{i}$, and $-5 - 6\mathrm{i}$ as illustrated in Figure 7. These loops generate the transposition $\sigma_{\gamma_1} = (3, 4)$ and the 4-cycle $\sigma_{\gamma_2} = (1, 4, 3, 2)$ showing that $M_\pi = S_4$. Hence, all four solutions, and notably z_1^*, can freely permute with each other over the complex numbers.

Now, we turn to the real case to contrast with the structure of the complex numbers. Let $Y = \mathbb{R}^3$, $U = \mathbb{R}^5 \times Y = \mathbb{R}^8$, and $\pi(x, \lambda, u) = u$ be as above. From u^*, we know that $d = 4$ is a typical number of solutions and there is a unique smoothly connected component $C_4 \subset Y_4$ which contains u^*. Let $h = \det J_z f$ where $z = (x, \lambda)$. Since $h(z_1^*, u^*)$ and $h(z_3^*, u^*)$ are positive while $h(z_2^*, u^*)$ and $h(z_4^*, u^*)$ are negative, this immediately yields that the real monodromy action could possibly only occur between z_1^* and z_3^*, and between z_2^* and z_4^*. We compute the connected components of $V_{\mathbb{R}}(f) \backslash V_{\mathbb{R}}(h)$ using a routing function approach with $c = (7/6, 2/3, -7/6, 4/5, -4/7, 7/4, 1/3, -1/6)$ where the variables are listed as (x, λ, u). This yields 10 routing points, 5 with $h > 0$ and 5 with $h < 0$. In particular, for both $h > 0$ and $h < 0$, there are four routing points with index 0 and one routing point with index 1 which connects to two different routing points of index 0. Thus, both $V_{\mathbb{R}}(f) \cap \{h > 0\}$ and $V_{\mathbb{R}}(f) \cap \{h < 0\}$ consist of three connected components with all components having Euler characteristic 1. Membership testing shows that (z_1^*, u^*) and (z_3^*, u^*) lie on different connected components of $V_{\mathbb{R}}(f) \cap \{h > 0\}$ while (z_2^*, u^*) and (z_4^*, u^*) lie on the same connected component of $V_{\mathbb{R}}(f) \cap \{h < 0\}$. Hence, $\mathcal{G}_{\pi, C_4, 1}$ is as follows:

– $\{1\} \mapsto \{\{1\}\}$

– $\{3\} \mapsto \{\{3\}\}$

– $\{2\}, \{4\} \mapsto \{\{2\}, \{4\}\}$.

In particular, $\mathcal{G}_{\pi, C_4, 1}$ shows that z_1^* and z_3^* have no nontrivial real monodromy action. Conversely, solutions z_2^* and z_4^* over u^* can be smoothly connected to each other via a loop in $\mathbb{R}^3$. This is in contrast to the complex monodromy group being S_4 so that all four solutions, including the statistically-meaningful solution z_1^*, can freely permute with each other over loops in $\mathbb{C}^3$.

5.2 Kuramoto model

The Kuramoto model [18] is an illustrative dynamical system to model synchronous behavior of coupled oscillators. The following considers the first tier of the real monodromy structure for steady-states for $n = 3$ (Section 5.2.1) and $n = 4$ (Section 5.2.2) oscillators. The real monodromy structure for the $n = 3$ case, which has a two-dimensional parameter space, was computed in [8, § 3].

5.2.1 3-oscillator model

For the $n = 3$ case, the steady-states for the Kuramoto model are described by the solutions to the polynomial system

$$f(c, s, \omega) = \begin{bmatrix} (s_1c_2 - c_1s_2) + (s_1c_3 - c_1s_3) - 3\omega_1 \\ (s_2c_1 - c_2s_1) + (s_2c_3 - c_2s_3) - 3\omega_2 \\ c_1^2 + s_1^2 - 1 \\ c_2^2 + s_2^2 - 1 \end{bmatrix}$$

where ω_j is the natural frequency of the j^{th} oscillator which is located at (c_j, s_j) on the unit circle with $(c_s, s_3) = (1, 0)$ and $\omega_3 = -(\omega_1 + \omega_2)$. The number of solutions for $f(c, s, \omega^*) = 0$ for generic $\omega^* \in \mathbb{C}^2$ is 6. As in [8, § 3], we consider $\omega^* = (0, 0)$ and label the six real solutions with $z = (c, s)$ as

$$z_1^* = (1, 1, 0, 0), \qquad z_2^* = (1, -1, 0, 0), \qquad z_3^* = (-1, 1, 0, 0), \qquad z_4^* = (-1, -1, 0, 0),$$
$$z_5^* = \tfrac{1}{2}(-1, -1, \sqrt{3}, -\sqrt{3}), \qquad z_6^* = \tfrac{1}{2}(-1, -1, -\sqrt{3}, \sqrt{3}).$$

Let $Y = \mathbb{C}^2$, $U = \mathbb{C}^4 \times Y = \mathbb{C}^6$, and $X = V_{\mathbb{C}}(f)$, whose irreducibility follows immediately from the irreducibility of the complex unit circle. For the projection map $\pi(c, s, \omega) = \omega$, the monodromy group M_π is equal to S_6 as summarized in [8, Ex. 3.4]. Hence, all six solutions can freely permute with each other over the complex numbers.

For the real case, let $Y = \mathbb{R}^2$, $U = \mathbb{R}^4 \times Y = \mathbb{R}^6$, and $\pi(c, s, \omega) = \omega$ as above. Solving at $\omega^* = (0, 0)$ shows that $d = 6$ is a typical number of solutions and there is a unique smoothly connected component $C_6 \subset Y_6$ which contains ω^*. Let $h = \det J_z f$ where $z = (c, s)$. Since $h(z_1^*, \omega^*)$, $h(z_5^*, \omega^*)$, $h(z_6^*, \omega^*) > 0$ while $h(z_2^*, \omega^*)$, $h(z_3^*, \omega^*)$, $h(z_4^*, \omega^*) < 0$, this immediately yields that the real monodromy action could possibly only occur amongst z_1^*, z_5^*, z_6^* and amongst z_2^*, z_3^*, z_4^*.

We compute the connected components of $V_{\mathbb{R}}(f) \backslash V_{\mathbb{R}}(h)$ using a routing function approach with randomly selected point $(0.73, 0.32, -0.12, 0.93, -0.27, 0.61)$ where the variables are listed as (c, s, ω). This yields 10 routing points, 3 with $h > 0$ and 7 with $h < 0$. For $h > 0$, the three routing points all have index 0, showing that $V_{\mathbb{R}}(f) \cap \{h > 0\}$ has three connected components each with Euler characteristic 1. Membership testing shows that (z_1^*, ω^*), (z_5^*, ω^*), and (z_6^*, ω^*) all lie on different connected components. For $h < 0$, there are two routing points with index 0 and five routing points with index 1. A routing road map shows that all lie on the same connected component so that $V_{\mathbb{R}}(f) \cap \{h < 0\}$ is connected with Euler characteristic -3 and contains (z_2^*, ω^*), (z_3^*, ω^*), and (z_4^*, ω^*). Hence, $\mathcal{G}_{\pi, C_6, 1}$ is as follows:

- $\{1\} \mapsto \{\{1\}\}$
- $\{2\}, \{3\}, \{4\} \mapsto \{\{2\}, \{3\}, \{4\}\}$
- $\{5\} \mapsto \{\{5\}\}$
- $\{6\} \mapsto \{\{6\}\}$

which is in agreement with [8, Ex. 3.15].

5.2.2 4-oscillator model

For the $n = 4$ case, we consider

$$f(c,s,\omega) = \begin{bmatrix} (s_1c_2 - c_1s_2) + (s_1c_3 - c_1s_3) + (s_1c_4 - c_1s_4) - 4\omega_1 \\ (s_2c_1 - c_2s_1) + (s_2c_3 - c_2s_3) + (s_3c_4 - c_3s_4) - 4\omega_2 \\ (s_3c_1 - c_3s_1) + (s_3c_2 - c_3s_2) + (s_3c_4 - c_3s_4) - 4\omega_3 \\ c_1^2 + s_1^2 - 1 \\ c_2^2 + s_2^2 - 1 \\ c_3^2 + s_3^2 - 1 \end{bmatrix}$$

where $(c_4, s_4) = (1, 0)$ and $\omega_4 = -(\omega_1 + \omega_2 + \omega_3)$. Although $f(c, s, \omega^*) = 0$ has 14 solutions for generic $\omega^* \in \mathbb{C}^3$, it was proven in [7, Thm. 4.1] that the maximum number of isolated real solutions is 10. We take $\omega^* = (0.2, 0.2, -0.198)$ where $f(c, s, \omega^*) = 0$ has 10 real solutions and two pairs of complex conjugate solutions.

Let $Y = \mathbb{C}^3$, $U = \mathbb{C}^6 \times Y = \mathbb{C}^9$, and $X = V_{\mathbb{C}}(f)$ which is irreducible. For the projection map $\pi(c, s, \omega) = \omega$, the monodromy group M_π is S_{14}. This can be observed using the two triangular loops $\gamma_j \subset \mathbb{C}^3$ with vertices listed in the following table.

loop	vertex 1	vertex 2	vertex 3
1	ω^*	$(4.61 + 3.69\mathrm{i}, -0.92 - 1.69\mathrm{i}, 4.56 - 2.97\mathrm{i})$	$(-1.55 - 4.86\mathrm{i}, -2.37 - 0.72\mathrm{i}, 3.03 + 3.20\mathrm{i})$
2	ω^*	$(-3.13 + 3.39\mathrm{i}, -3.69 - 3.02\mathrm{i}, 3.02 + 4.65\mathrm{i})$	$(-3.56 + 0.36\mathrm{i}, -0.71 - 0.32\mathrm{i}, -0.21 + 2.23\mathrm{i})$

Labeling the solutions as

$$\begin{array}{rcl}
z_1^* &=& (\ 0.9157,\ 0.9157,\ 1.0000,\ 0.4019,\ 0.4019,\ 0.0042), \\
z_2^* &=& (-0.6151, -0.9998,\ 0.9992,\ 0.7884, -0.0204,\ 0.0400), \\
z_3^* &=& (-0.9998, -0.6151,\ 0.9992, -0.0204,\ 0.7884,\ 0.0400), \\
z_4^* &=& (-0.9998, -0.9998,\ 0.6453,\ 0.0220,\ 0.0220,\ 0.7639), \\
z_5^* &=& (-0.5745, -0.5745,\ 0.5593,\ 0.8185,\ 0.8185, -0.8289), \\
z_6^* &=& (\ 0.5960, -1.0000,\ 0.9999,\ 0.8030, -0.0050,\ 0.0100), \\
z_7^* &=& (-1.0000,\ 0.5960,\ 0.9999, -0.0050,\ 0.8030,\ 0.0100), \\
z_8^* &=& (-0.9346, -0.9346,\ 0.9953,\ 0.3556,\ 0.3556,\ 0.0968), \\
z_9^* &=& (-1.0000, -1.0000, -0.6026,\ 0.0050,\ 0.0050,\ 0.7980), \\
z_{10}^* &=& (\ 0.5933,\ 0.5933, -0.5973,\ 0.8050,\ 0.8050, -0.8020), \\
\hline
z_{11}^* &=& (-1.0000 + 0.0000\mathrm{i},\ 2.0095 - 80.8189\mathrm{i}, -1.9996 + 80.0107\mathrm{i}, \\
&& \quad -0.0001 - 0.0099\mathrm{i},\ 80.8251 + 2.0094\mathrm{i}, -80.0170 - 1.9994\mathrm{i}), \\
z_{12}^* &=& (-1.0000 - 0.0000\mathrm{i},\ 2.0095 + 80.8189\mathrm{i}, -1.9996 - 80.0107\mathrm{i}, \\
&& \quad -0.0001 + 0.0099\mathrm{i},\ 80.8251 - 2.0094\mathrm{i}, -80.0170 + 1.9994\mathrm{i}), \\
z_{13}^* &=& (\ 2.0095 + 80.8189\mathrm{i}, -1.0000 - 0.0000\mathrm{i}, -1.9996 - 80.0107\mathrm{i}, \\
&& \quad 80.8251 - 2.0094\mathrm{i}, -0.0001 + 0.0099\mathrm{i}, -80.0170 + 1.9994\mathrm{i}), \\
z_{14}^* &=& (\ 2.0095 - 80.8189\mathrm{i}, -1.0000 + 0.0000\mathrm{i}, -1.9996 + 80.0107\mathrm{i}, \\
&& \quad 80.8251 + 2.0094\mathrm{i}, -0.0001 - 0.0099\mathrm{i}, -80.0170 - 1.9994\mathrm{i}),
\end{array}$$

the corresponding permutations are

$$\sigma_{\gamma_1} = (1, 10, 7, 12, 8, 4, 9, 3, 5, 11)(2, 6, 13) \quad \text{and} \quad \sigma_{\gamma_2} = (2, 3, 13, 10, 14, 12)(8, 11, 9).$$

`Mathematica` confirms $\langle \sigma_{\gamma_1}, \sigma_{\gamma_2} \rangle = S_{14}$. Hence, over the complex numbers, all 14 solutions can freely permute with each other.

For the real case, let $Y = \mathbb{R}^3$, $U = \mathbb{R}^6 \times Y = \mathbb{R}^{10}$, and $\pi(c, s, \omega) = \omega$ as above. Solving at $\omega^* = (0.2, 0.2, -0.198)$ shows that $d = 10$ is a typical number of solutions and there is a unique smoothly connected component $C_{10} \subset Y_{10}$ which contains ω^*. Let $h = \det J_z f$ where $z = (c, s)$. Since $h(z_1^*, \omega^*), \ldots, h(z_5^*, \omega^*) < 0$ while $h(z_6^*, \omega^*), \ldots, h(z_{10}^*, \omega^*) > 0$, this immediately yields that the real monodromy action could possibly only occur amongst $z_1^*, \ldots, z_5^*$ and amongst $z_6^*, \ldots, z_{10}^*$.

We compute the connected components of $V_{\mathbb{R}}(f) \backslash V_{\mathbb{R}}(h)$ using a routing function approach with randomly selected point $(0.73, 0.32, -0.12, 0.93, -0.27, 0.61, 0.82, -0.11, 0.94)$ where the variables are listed as (c, s, ω). This yields 49 routing points, 16 with $h > 0$ and 33 with $h < 0$. For $h > 0$, four routing points have index 0, nine have index 1, and three have index 2 to total 16. A routing road map shows that all lie on the same connected component yielding that $V_{\mathbb{R}}(f) \cap \{h > 0\}$ is connected with Euler characteristic $-2 = 4-9+3$ and contains $(z_6^*, \omega^*), \ldots, (z_{10}^*, \omega^*)$. For $h < 0$, 11 routing points have index 0 and 22 have index 1. A routing road map shows that $V_{\mathbb{R}}(f) \cap \{h < 0\}$ has two connected components. One of the connected components contains (z_1^*, ω^*) and has a single routing point of index 0, showing that it has Euler characteristic 1. The other connected component, which contains $(z_2^*, \omega^*), \ldots, (z_5^*, \omega^*)$, has 10 routing points of index 0 and 22 routing points of index 1 showing that it has Euler characteristic -12. Hence, $\mathcal{G}_{\pi, C_{10}, 1}$ is as follows:

- $\{1\} \mapsto \{\{1\}\}$
- $\{2\}$, $\{3\}$, $\{4\}$, $\{5\} \mapsto \{\{2\}, \{3\}, \{4\}, \{5\}\}$
- $\{6\}$, $\{7\}$, $\{8\}$, $\{9\}$, $\{10\} \mapsto \{\{6\}, \{7\}, \{8\}, \{9\}, \{10\}\}$.

In particular, z_1^* in both the $n = 3$ and $n = 4$ case is the unique solution where all of the c_j's are positive and has only trivial real monodromy action.

5.3 3RPR mechanism

The 3RPR mechanism is a planar parallel manipulator consisting of a moving platform that is connected to ground via three prismatic (P) legs with rotational (R) joints on both ends as illustrated in Figure 8. The position and orientation of the moving platform is controlled by adjusting the leg lengths. It is well-known that this mechanism has a nonsingular assembly mode change, e.g., see [15, 16, 19, 26]. That is, treating the leg lengths as parameters, the position and orientation of the moving platform can have nontrivial first tier of the real monodromy structure.

After formulating the polynomial system in isotropic coordinates (Section 5.3.1), six different instances are considered: two leg lengths free (Section 5.3.2), three leg lengths free (Section 5.3.3), imposing leg length restrictions (Section 5.3.4), avoiding wall and floor obstacles (Section 5.3.5), imposing leg length restrictions while also avoiding wall and floor obstacles (Section 5.3.6), and finally one with only trivial real monodromy action (Section 5.3.7).

5.3.1 Isotropic formulation

An efficient approach to describe planar mechanisms such as the 3RPR mechanism is by using isotropic coordinates. In short, points (x, y) written in Cartesian coordinates in the plane correspond with points $(z, \bar{z})$ written in isotropic coordinates with $z = x + \mathrm{i}y$ and $\bar{z} = x - \mathrm{i}y$ where $\mathrm{i} = \sqrt{-1}$. Hence, $(x, y) \in \mathbb{R}^2$ if and only if the corresponding point $(z, \bar{z})$ in isotropic coordinates satisfies $\bar{z} = \mathrm{conj}(z)$ where conj() is the complex conjugate. In particular, one can replace "real"

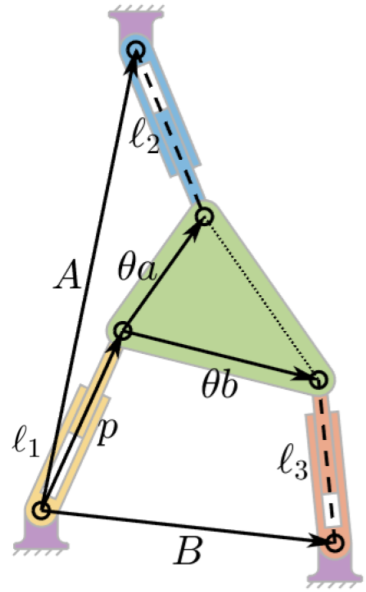

Figure 8: A schematic of a 3RPR mechanism.

computations in Cartesian coordinates with "isotropically real" computations in isotropic coordinates, e.g., see [10] for performing routing road map computations with isotropic coordinates. Therefore, throughout the rest of this section, we just use the word real to mean isotropically real.

With respect to the fixed frame, as illustrated in Figure 8, let $(A, \bar{A})$ and $(B, \bar{B})$ denote the offsets from the first fixed pivot to the second and third fixed pivots, respectively. In the moving frame, $(a, \bar{a})$ and $(b, \bar{b})$ play similar roles. The position of the moving frame with respect to the fixed frame is described by translation $(p, \bar{p})$ and rotation $(\theta, \bar{\theta})$ which satisfies the Pythagorean identity in isotropic coordinates, namely $\theta \cdot \bar{\theta} = 1$. Although the j^{th} leg length is denoted by ℓ_j, only square lengths appear so we will consider $c_j = \ell_j^2$. With this, the polynomial system for the 3RPR mechanism in isotropic coordinates is:

$$f = \begin{bmatrix} p \cdot \bar{p} - c_1, \\ (p + a \cdot \theta - A) \cdot (\bar{p} + \bar{a} \cdot \bar{\theta} - \bar{A}) - c_2 \\ (p + b \cdot \theta - B) \cdot (\bar{p} + \bar{b} \cdot \bar{\theta} - \bar{B}) - c_3 \\ \theta \cdot \bar{\theta} - 1 \end{bmatrix}. \tag{17}$$

In particular, the first three polynomials are the leg length conditions for the three legs, respectively, and the last is the Pythagorean identity.

Corresponding to the case studied in [8, 15], we fix

$$a = \bar{a} = 7/5, \quad b = 7/10 + \mathrm{i}, \quad \bar{b} = 7/10 - \mathrm{i}, \quad A = \bar{A} = 8/5, \quad B = 9/10 + 3\mathrm{i}/5, \quad \bar{B} = 9/10 - 3\mathrm{i}/5,$$

and consider f as a polynomial system in variables $z = (p, \bar{p}, \theta, \bar{\theta})$ and parameters $c = (c_1, c_2, c_3)$ yielding projection map $\pi(p, \bar{p}, \theta, \bar{\theta}, c_1, c_2, c_3) = (c_1, c_2, c_3)$. The generic number of solutions is 6 and, for $c^* = (c_1^*, c_2^*, c_3^*) = (0.75, 0.7, 1)$, all six solutions are real which are labeled as in Figure 9.

Consider $Y = \mathbb{C}^4$, $U = \mathbb{C}^3 \times Y = \mathbb{C}^7$, and $X = V_{\mathbb{C}}(f)$, whose irreducibility immediately follows from the irreducibility of the Pythagorean identity. The monodromy group is $M_\pi = S_6$ which can be observed fixing $c_2 = c_2^*$ and $c_3 = c_3^*$ and letting c_1 vary along the triangular loops with vertices listed in the following table.

loop	vertex 1	vertex 2	vertex 3
1	c_1^*	$-2.11 - 0.37\mathrm{i}$	$2.36 + 4.27\mathrm{i}$
2	c_1^*	$-3.14 + 2.79\mathrm{i}$	$4.33 - 3.34\mathrm{i}$

Although the monodromy group over the complex numbers is the full symmetric group, the following six different instances demonstrate various real monodromy action. For $h = \det J_z f$, $h > 0$ for solutions $1, 2, 3$ and $h < 0$ for solutions $4, 5, 6$. Hence, real monodromy action could possibly only occur amongst z_1^*, z_2^*, z_3^* and z_4^*, z_5^*, z_6^*.

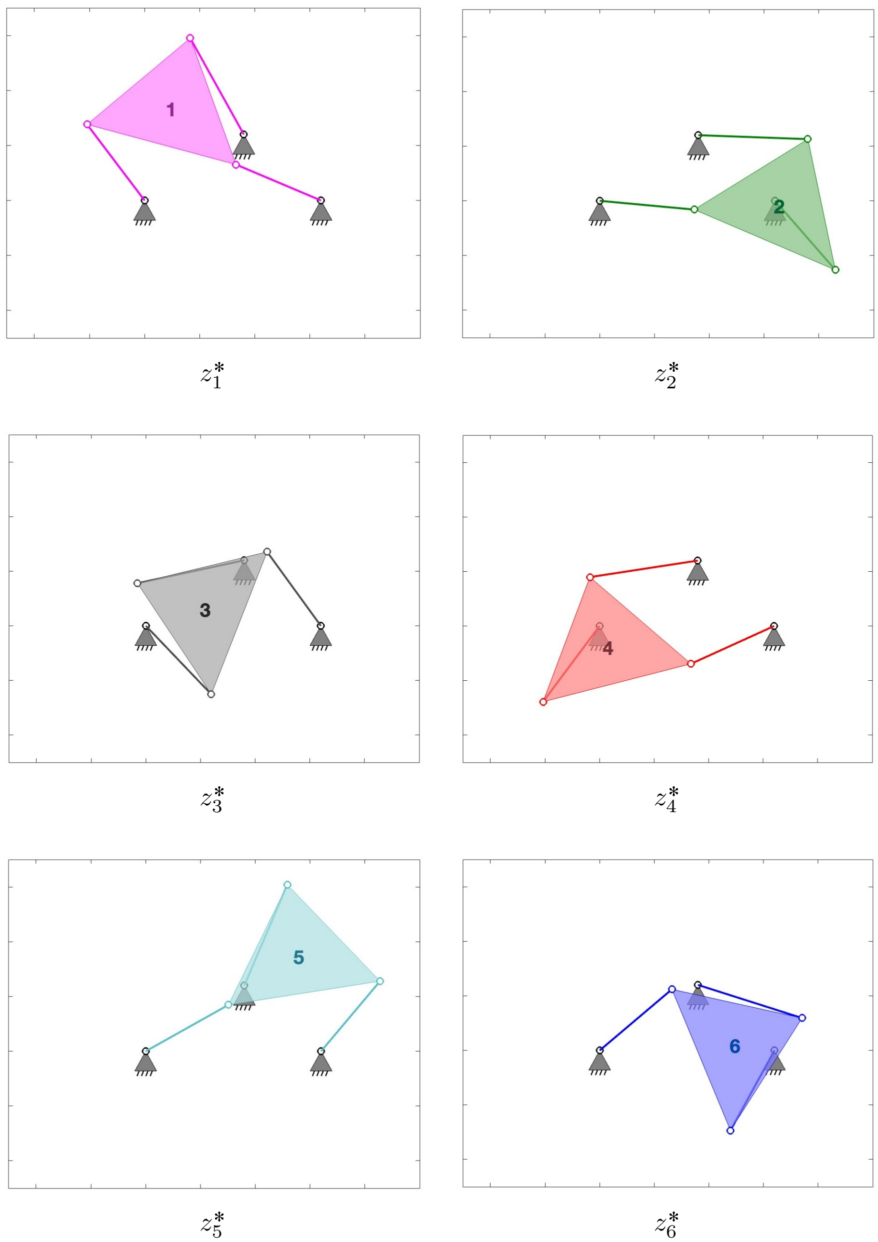

Figure 9: Labeling six solutions to the 3RPR mechanism

5.3.2 Two legs free

Since the brute force computational approach described in [8, Alg. 1] was limited to $\mathbb{R}^2$, [8, § 4] considered real monodromy action for the 3RPR mechanism where one of the three leg lengths was fixed and the other other two were free to change lengths. Fixing $c_3 = c_3^*$, we verified that the first tier of the real monodromy structure using Algorithm 3 is indeed

- $\{1\}, \{2\}, \{3\} \mapsto \{\{1\}, \{2\}, \{3\}\}$
- $\{4\}, \{5\}, \{6\} \mapsto \{\{4\}, \{5\}, \{6\}\}$

when, as usual using the abuse of notation for isotropically real, taking $Y = \mathbb{R}^4$, $U = \mathbb{R}^2 \times Y = \mathbb{R}^6$, and $X = V_{\mathbb{R}}(f)$. In our computation, there were 12 routing points with a routing road map yielding two smoothly connected components that just happen to correspond with $V_{\mathbb{R}}(f) \cap \{h > 0\}$ and $V_{\mathbb{R}}(f) \cap \{h < 0\}$. In particular, $V_{\mathbb{R}}(f) \cap \{h > 0\}$ contained five routing points, three of index 0 and two of index 1, as well as (z_j^*, c_1^*, c_2^*) for $j = 1, 2, 3$. Additionally, $V_{\mathbb{R}}(f) \cap \{h < 0\}$ contained seven routing points, three of index 0 and four of index 1, as well as (z_j^*, c_1^*, c_2^*) for $j = 4, 5, 6$.

5.3.3 Three legs free

Since Algorithm 3 is not limited to $\mathbb{R}^2$, one can allow all three leg lengths to vary when taking $Y = \mathbb{R}^4$, $U = \mathbb{R}^3 \times Y = \mathbb{R}^7$, and $X = V_{\mathbb{R}}(f)$. This computation also determines that $V_{\mathbb{R}}(f) \cap \{h > 0\}$ and $V_{\mathbb{R}}(f) \cap \{h < 0\}$ are both smoothly connected yielding the same first tier as in Section 5.3.2. Our computation yielded 20 routing points with each smoothly connected component consisting of three of index 0 and seven of index 1. Figure 10 provides a visualization of a connection between z_4^* and z_5^* and a connection between z_4^* and z_6^* with the path in the images tracing out the location of p.

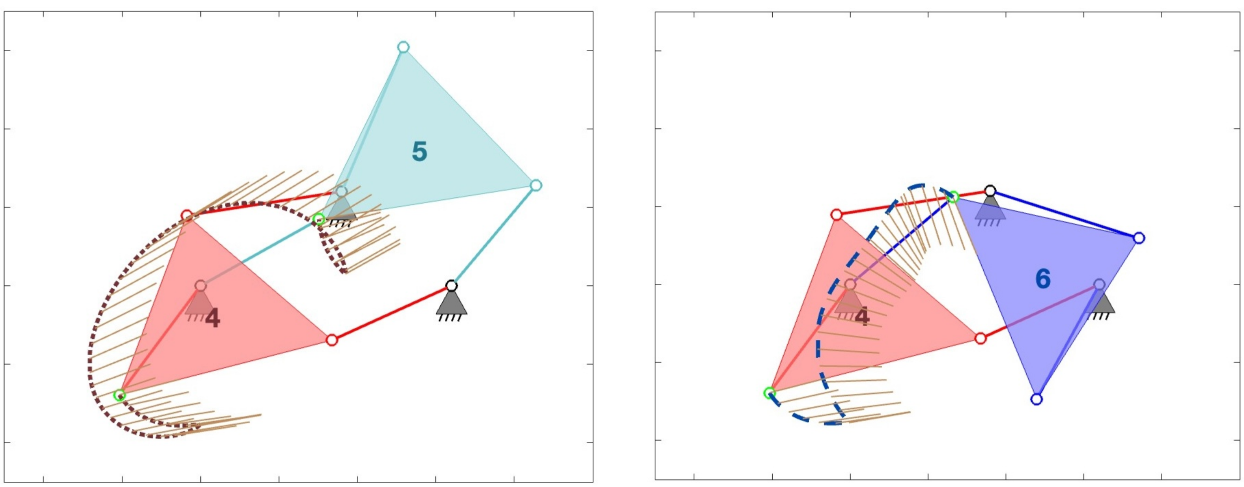

(a) Connection between z_4^* (red) and z_5^* (cyan)

(b) Connection between z_4^* (red) and z_6^* (blue)

Figure 10: Illustrating nonsingular assembly mode changes between z_4^*, z_5^*, and z_6^*

5.3.4 Leg length restrictions

From an engineering perspective, there are additional constraints that we can impose to make our model more practical. Here, we consider the case where all of the leg lengths are constrained between a minimum and maximum length. In particular, for $\phi = 0.75$, we impose that $\ell_j \in (\phi, 2\phi)$ for $j = 1, 2, 3$. Since $c_j = \ell_j^2$, let $\mu = \phi^2 = 0.5625$ so this restriction translates to a parameter space restriction of $c_j \in (\mu, 4\mu)$ for $j = 1, 2, 3$. Hence, we take $Y \subset \mathbb{R}^3$ to be smoothly connected semialgebraic set defined by

$$Y = (\mu, 4\mu)^3 = \{c \in \mathbb{R}^3 \mid c_j - \mu > 0 \text{ and } 4\mu - c_j > 0 \text{ for } j = 1, 2, 3\}.$$

With $U = \mathbb{R}^4 \times Y$, the restriction of $X \subset V_U(f)$ imposes six linear inequality constraints that yield a product of six linears in the numerator of our routing function, one for each side of the bound for each of the three legs. With these leg length restrictions, the first tier of the real monodromy structure using Algorithm 3 is

- $\{1\}, \{2\} \mapsto \{\{1\}, \{2\}\}$
- $\{3\} \mapsto \{\{3\}\}$
- $\{4\}, \{5\} \mapsto \{\{4\}, \{5\}\}$
- $\{6\} \mapsto \{\{6\}\}$

In our computation, there were 10 routing points with a routing road map yielding four smoothly connected components. The smoothly connected component containing (z_1^*, c^*) and (z_2^*, c^*) as well as the one containing (z_4^*, c^*) and (z_5^*, c^*) contained four routing points, two of index 0 and two of index 1. Additionally, the one containing (z_3^*, c^*) as well as the one containing (z_6^*, c^*) had only had one routing point which had index 0.

Since it was not prescribed *a priori*, it is not a surprise that the two paths illustrated in Figure 10 fail the leg length restrictions. For example, the path in Figure 10b moves close to the fixed pivot meaning that first leg length becomes quite small along the path. The first tier of the real monodromy structure above shows that it is not possible create a path that satisfies the leg length restrictions between z_4^* and z_6^*. Conversely, the path in Figure 10a between z_4^* and z_5^* can be replaced with one that does satisfy the leg length restrictions as shown in Figure 11. In this figure, a gray circle illustrates the minimum leg length restriction for the first leg with the path in Figure 10a intersecting this circle while the newly constructed path remains outside of this circle.

5.3.5 Wall and floor obstacles

Another type of constraint is to ensure that the mechanism avoids a wall and a floor. In Cartesian coordinates, we place the wall at $x = -0.6$ and the floor at $y = -0.75$. Therefore, we require each vertex of the three rotational joint locations on the moving platform to be in $(-0.6, \infty) \times (-0.75, \infty)$ in Cartesian coordinates with respect to the fixed frame. For example, the rational joint for the first leg is at $(p, \bar{p})$ in isotropic coordinates so this translates to $x = (p + \bar{p})/2 > -0.6$ and $y = (p - \bar{p})/(2\mathrm{i}) > -0.75$. Similar inequalities are easily derived for the other two legs yielding a total of six linear equality constraints. In particular, since the leg lengths themselves are not restricted, we have $Y = \mathbb{R}^3$ while $U \subset \mathbb{R}^4 \times Y = \mathbb{R}^7$ is defined by these six linear inequality constraints. Hence, the restriction of $X \subset V_U(f)$ also yields a product of six linears in the numerator of our routing function. Since all six of the solutions illustrated in Figure 9 properly satisfy the wall and floor inequality constraints, Algorithm 3 with $d = 6$ yields that the first tier of the real monodromy structure is

- $\{1\}, \{2\}, \{3\} \mapsto \{\{1\}, \{2\}, \{3\}\}$
- $\{4\}, \{5\}, \{6\} \mapsto \{\{4\}, \{5\}, \{6\}\}$.

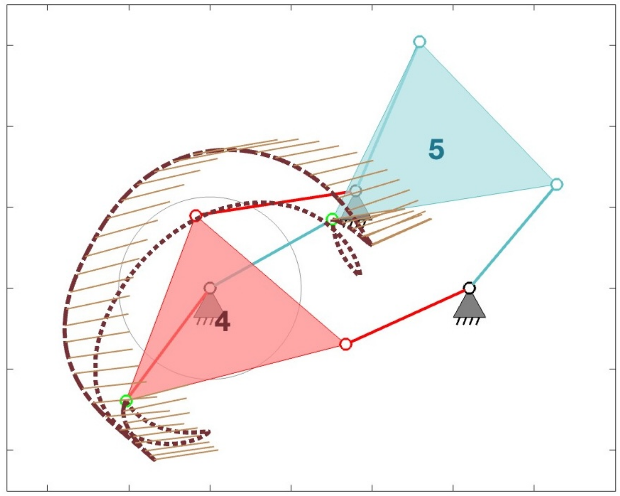

Figure 11: Illustrating a nonsingular assembly mode change between z_4^* (red) and z_5^* (cyan) that satisfies the leg length restrictions along with the path from Figure 10a that does not satisfy the leg length restrictions. The gray circle represents the minimum leg length constraint for the first leg.

In our computation, there were 18 routing points with two smoothly connected components, one contained in $\{h > 0\}$ and the other in $\{h < 0\}$, each consisting of 9 routing points, 3 of index 0 and 6 of index 1.

Although this first tier is the same as when two legs (Section 5.3.2) and three legs (Section 5.3.3) are free, the paths between the configurations are altered to avoid hitting the wall and floor obstacles. Figure 12 shows the newly computed paths between z_4^* and z_5^* as well as z_4^* and z_6^*.

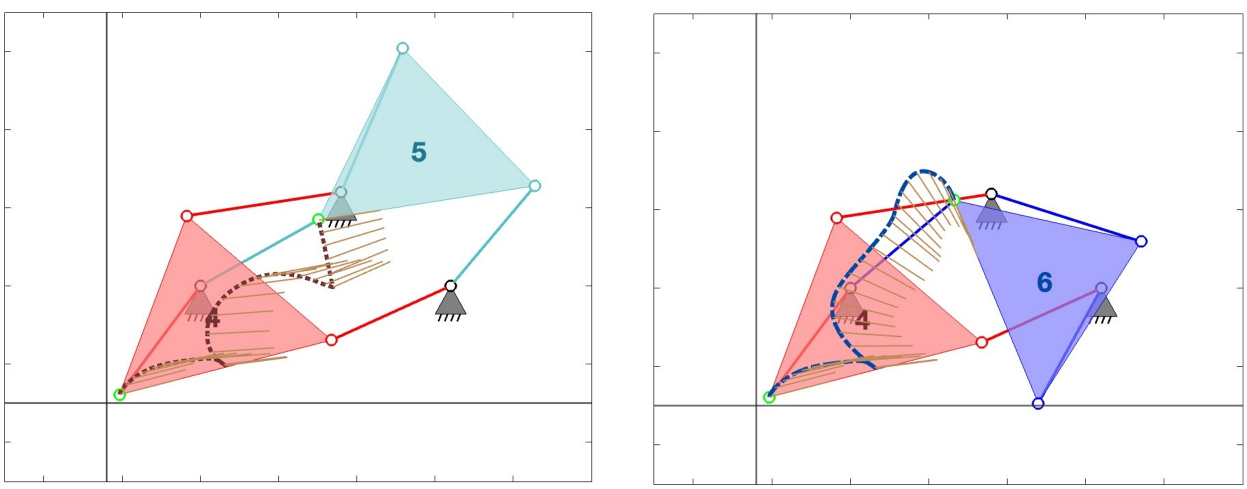

(a) Connection between z_4^* (red) and z_5^* (cyan)

(b) Connection between z_4^* (red) and z_6^* (blue)

Figure 12: Illustrating nonsingular assembly mode changes between z_4^*, z_5^*, and z_6^* that keep the moving platform away from the wall and floor boundaries (shown as gray lines).

5.3.6 Leg length restrictions along with wall and floor obstacles

We can impose both the leg length restrictions from Section 5.3.4 and wall and floor avoidance from Section 5.3.5. This yields a total of 12 additional linear inequality constraints and the following first tier of the real monodromy structure:

- $\{1\}, \{2\} \mapsto \{\{1\}, \{2\}\}$
- $\{m_1\} \mapsto \{\{m_1\}\}$ for all others

Hence, the only nonsingular assembly mode change that remains is between z_1^* and z_2^* as illustrated in Figure 13. Our computation produced 9 routing points and 7 smoothly connected components. Six of the smoothly connected components had only one routing point, which had index 0, with four of these containing one of (z_j^*, c^*) for $j = 3, \ldots, 6$. The seventh smoothly connected component had 3 routing points, two of index 0 and one of index 1, and contained both (z_1^*, c^*) and (z_2^*, c^*).

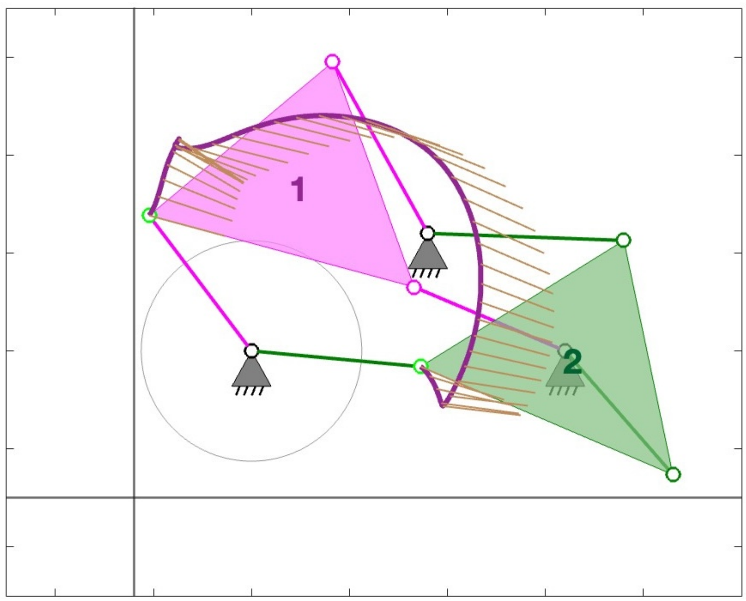

Figure 13: Illustrating nonsingular assembly mode change between z_1^* (pink) and z_2^* (green) maintaining leg length restrictions and avoiding wall and floor boundaries. The gray circle represents the minimum leg length constraint for the first leg and the gray lines are the wall and floor boundaries.

5.3.7 Cutting off real monodromy

Since Section 5.3.6 showed that imposing both the leg length restrictions from Section 5.3.4 and wall and floor avoidance from Section 5.3.5 still had a nonsingular assembly mode change, we need to impose more restrictive conditions to only have trivial real monodromy action. For example, considering keeping the same wall and floor obstacles as in Section 5.3.5 but restricting the leg length constraints to $\tilde{\mu} < c_j < 1.9\tilde{\mu}$ for $j = 1, 2, 3$ where $\tilde{\mu} = 0.64$. Then, each point (z_j^*, c^*) for $j = 1, \ldots, 6$ lies on distinct smoothly connected components yielding trivial real monodromy action. In our computation, each of the distinct smoothly connected component was represented by a single routing point of index 0.

6 Conclusion

The Galois/monodromy group over the complex numbers is well-studied and provides insight into structure associated with a branched covering. Since the real monodromy group is often trivial due to simultaneously considering all real solutions, the real monodromy structure was introduced in [8] to capture tiered behavior of the real solutions. Since [8, Alg. 1] was restricted to computing real monodromy structures over a two-dimensional parameter space, a fiber product inspired approach was developed in Theorem 3.10 and Algorithm 3 for computing real monodromy structures. This new computational approach depends upon testing membership in smoothly connected components which is facilitated by routing functions [3, 13, 14]. Examples in algebraic statistics, dynamical systems, and kinematics demonstrate the new approach. Since one downside of using fiber products is the growth of the size of the polynomial systems involved, future research includes developing new computational approaches to take advantage of the structure of fiber products to reduce computational costs.

Acknowledgments

The authors thank Joe Cummings for discussions regarding routing function computations.

References

[1] D. J. Bates, J. D. Hauenstein, A. J. Sommese, and C. W. Wampler. Bertini: Software for numerical algebraic geometry. Available at `bertini.nd.edu`.

[2] D. J. Bates, J. D. Hauenstein, A. J. Sommese, and C. W. Wampler. *Numerically Solving Polynomial Systems with Bertini*, volume 25 of *Software, Environments, and Tools*. Society for Industrial and Applied Mathematics (SIAM), Philadelphia, PA, 2013.

[3] J. Cummings, J. D. Hauenstein, H. Hong, and C. D. Smyth. Smooth connectivity in real algebraic varieties. *Numer. Algorithms*, 100(1):63–84, 2025.

[4] P. B. Edwards and J. D. Hauenstein. On computing local monodromy and the numerical local irreducible decomposition. *Trans. London Math. Soc.*, 13(1):e70025, 2026.

[5] J. El Omri and P. Wenger. A general criterion for the identification of nonsingular posture changing 3-dof manipulators. In J.-P. Merlet and B. Ravani, editors, *Computational Kinematics '95*, pages 153–162, Dordrecht, 1995. Springer Netherlands.

[6] J. Harris. Galois groups of enumerative problems. *Duke Math. J.*, 46(4):685–724, 1979.

[7] K. Harris, J. D. Hauenstein, and A. Szanto. Smooth points on semi-algebraic sets. *J. Symb. Comput.*, 116:183–212, 2023.

[8] J. D. Hauenstein and M. H. Regan. Real monodromy action. *Appl. Math. Comput.*, 373:124983, 13, 2020.

[9] J. D. Hauenstein, J. I. Rodriguez, and F. Sottile. Numerical computation of Galois groups. *Found. Comput. Math.*, 18(4):867–890, 2018.

[10] J. D. Hauenstein, E. L. Schmidt, and C. W. Wampler. Routing functions for robot paths that avoid singularities and algebraic obstacles. To appear in *Advances in Robot Kinematics 2026 - Innovations in Motion: Shaping the Future of Robotic Systems.*

[11] J. D. Hauenstein and C. W. Wampler. Isosingular sets and deflation. *Found. Comput. Math.*, 13(3):371–403, 2013.

[12] C. Hermite. Sur les fonctions algébriques. *CR Acd. Sci. (Paris)*, 32:458–461, 1851.

[13] H. Hong. Connectivity in semi-algebraic sets. In *2010 12th International Symposium on Symbolic and Numeric Algorithms for Scientific Computing*, pages 4–7, 2010.

[14] H. Hong, J. Rohal, M. Safey El Din, and É. Schost. Connectivity in semi-algebraic sets I. arXiv:2011.02162, 2020.

[15] M. L. Husty. Non-singular assembly mode change in 3-RPR-parallel manipulators. In A. Kecskeméthy and A. Müller, editors, *Computational Kinematics*, pages 51–60, Berlin, Heidelberg, 2009. Springer Berlin Heidelberg.

[16] C. Innocenti and V. Parenti-Castelli. Singularity-free evolution from one configuration to another in serial and fully-parallel manipulators. *J. Mech. Des.*, 120(1):73–79, 1998.

[17] C. Jordan. *Traité des substitutions et des équations algébriques.* Gauthier-Villars, Paris, 1870.

[18] Y. Kuramoto. *Chemical oscillations, waves, and turbulence*, volume 19 of *Springer Series in Synergetics.* Springer-Verlag, Berlin, 1984.

[19] E. Macho, O. Altuzarra, C. Pinto, and A. Hernández. Singularity free change of assembly mode in parallel manipulators. Application to the 3-RPR planar platform. In *Proceedings of the 12th IFToMM World Congress*, pages Paper 801, 1–6, Besançon, France, June 2007.

[20] D. H. Myszka, A. P. Murray, and C. W. Wampler. Computing the branches, singularity trace, and critical points of single degree-of-freedom, closed-loop linkages. *J. Mech. Robot.*, 6(1):011006, 2014.

[21] J. I. Rodriguez and X. Tang. Data-discriminants of likelihood equations. In *Proceedings of the 2015 ACM International Symposium on Symbolic and Algebraic Computation*, ISSAC '15, page 307–314, New York, NY, USA, 2015. Association for Computing Machinery.

[22] A. J. Sommese, J. Verschelde, and C. W. Wampler. Symmetric functions applied to decomposing solution sets of polynomial systems. *SIAM J. Numer. Anal.*, 40(6):2026–2046, 2002.

[23] A. J. Sommese and C. W. Wampler. *The Numerical Solution of Systems of Polynomials Arising in Engineering and Science.* World Scientific Publishing Co. Pte. Ltd., Hackensack, NJ, 2005.

[24] A. J. Sommese and C. W. Wampler. Exceptional sets and fiber products. *Found. Comput. Math.*, 8(2):171–196, 2008.

[25] R. Vakil. Schubert induction. *Ann. of Math. (2)*, 164(2):489–512, 2006.

[26] M. Zein, P. Wenger, and D. Chablat. Non-singular assembly-mode changing motions for 3-RPR parallel manipulators. *Mech. Mach. Theory*, 43(4):480–490, 2008.